Kadanoff-Baym dynamics of Hubbard clusters: Performance of many-body schemes, correlation-induced damping and multiple steady and quasi-steady states

Marc Puig von Friesen, C. Verdozzi, and C.-O. Almbladh

Mathematical Physics and European Theoretical Spectroscopy Facility (ETSF), Lund University, 22100 Lund, Sweden

We present in detail a method we recently introduced [Phys. Rev. Lett. **103**, 176404 (2009)] to describe finite systems in and out of equilibrium, where the evolution in time is performed via the Kadanoff-Baym equations within many-body perturbation theory. Our systems consist of small, strongly correlated clusters, described by a Hubbard Hamiltonian within the Hartree-Fock, second Born, *GW*, and *T*-matrix approximations. We compare the results from the Kadanoff-Baym dynamics to those from exact numerical solutions. The outcome of our comparisons is that, among the many-body schemes considered, the *T*-matrix approximation is superior at low electron densities while none of the tested approximations stands out at half filling. Such comparisons permit a general assessment of the whole idea of applying many-body perturbation theory, in the Kadanoff-Baym sense, to finite systems. A striking outcome of our analysis is that when the system evolves under a strong external field, the Kadanoff-Baym equations develop a steady-state solution as a consequence of a correlation-induced damping. This damping is present both in isolated (finite) systems, where it is purely artificial, as well as in clusters contacted to (infinite) macroscopic leads. The extensive numerical characterization we performed indicates that this behavior is present whenever approximate self-energies, which include correlation effects, are used. Another important result is that, for isolated clusters, the steady state reached is not unique but depends on how one switches on the external field. When the clusters are coupled to macroscopic leads, one may reach multiple quasisteady states with arbitrarily long lifetimes.

I. INTRODUCTION

The Kadanoff-Baym equations (KBEs) (Refs. 1 and 2) are one of the fundamental theoretical schemes of a microscopic description of quantum systems out of equilibrium.[3,4] Due to the growing interest in time-dependent phenomena, in recent years the KBE have been the object of considerable attention in several branches of physics. Notable applications of the KBE are in the areas of molecular quantum transport, high-energy coupled plasmas, nuclear matter, astrophysics, to mention a few.[5–17] Another favorable element to the widespread use of KBE is the constantly expanding capability of today's computers, which has made the full numerical solution of the KBE possible. A main strength of the KBE is that one can, in a constructive way, build approximations of increasing complexity for the one-particle Green's function, *G*, the key quantity in the KBE. These approximations are obtained via many-body perturbation theory (MBPT) and are known as conserving approximations since they guarantee the conservation of important quantities such as total energy, number of particles, linear and angular momentum.

However, the fulfillment of such conserving conditions is no guarantee of the quality of the actual results obtained within a specific many-body approximation (MBA). Hence, it would be useful to have a way to assess the performance of a given conserving MBA. One of the aims of this paper is to evaluate the range of validity of a group of well-known MBAs by comparing the one-particle densities with the exact results for finite strongly correlated clusters out of equilibrium. The main attractive feature of such comparisons to exact results is the possibility of scrutinizing the performance of the MBAs in the nonequilibrium regime. This knowledge is most valuable if one wishes to use approximate many-body schemes for systems (typically, infinite ones, e.g., systems coupled to macroscopic leads as those we consider toward the end of the paper) where exact solutions are not available.

Describing small clusters with strong electronic correlations, and subject to time-dependent fields, presents interest not only from a conceptual point of view; there are very many instances where the technological relevance of cluster physics is manifestly evident.[18,19] The main focus of this work is to investigate the dynamics of finite clusters. In this regard, we provide here a detailed account of a study performed very recently,[17] producing additional results for clusters and presenting in great detail the methodology we developed. We will, however, present some results for a system contacted to macroscopic contacts to generalize some of our main findings. Similar clusters to those discussed here, coupled to leads have already been considered either in the stationary limit[11] or in the real-time domain.[13–15]

As specific finite model systems, we consider open-ended and ring-shaped short chains,[20] with local Hubbard interactions. We study their dynamics through exact diagonalization methods and by propagating the KBE for different MBAs. The approximations we consider are the Hartree-Fock approximation (HFA), the second Born approximation (BA), the *GW* approximation (GWA),[21] and the *T*-matrix approximation (TMA).[22,23] All these approximations are conserving,[1] which clearly is of great importance when propagating the KBE, and all of them, apart from HFA, have self-energies which are nonlocal in space and time. For the GWA, we will consider both a spin-independent and a spin-dependent version.[11,24] The latter has the advantage to alleviate the effect of self-screening.[25,26]

A general outcome of our study is that the TMA performs better than the other MBAs at low filling. At half filling, all

MBAs which involve correlation effects are of comparable quality. With the exact and KBE cluster dynamics at our disposal, we also investigate numerically a well-established relation between MBPT and another framework to treat non-equilibrium phenomena, i.e., time-dependent density-functional theory (TDDFT).[27,28] Using a spin-independent TDDFT description for the spin-compensated Hubbard model,[29] we will obtain the exchange-correlation (XC) potentials corresponding to the different MBAs via reverse engineering from the time-dependent densities. While the topic of TDDFT appears to be somewhat peripheral to the main aim of this work, we wish to remark that finding good approximations for TDDFT is of major importance as this method is a much more suitable candidate for treating real systems as the quantities involved depend only on one time coordinate.

Our results show that the time-dependent KBE present two interesting features. The first is that for large external fields, the KBE time evolution in clusters exhibits a damped behavior induced by many-body correlations (hereafter, we refer to this as correlation-induced damping). The second feature is that the steady state one reaches in an isolated cluster is not unique but depends on how the perturbation is switched on. We also investigate clusters connected to macroscopic leads, which we in this paper treat within the TMA and BA. In this case, the correlation-induced damping is also present. Moreover, if there are sharp resonances outside the band continuum, the KBE will give rise to multiple quasi-steady states, i.e., long-lived states which can take arbitrary long time to decay to the true steady state.

In finite clusters, the correlation-induced damping and the existence of multiple steady states is artificial and we show that it is due to limitations of self-consistent many-body perturbation theory when applied to finite systems.

The question whether or not the correlation-induced damping and the existence of multiple quasisteady states in contacted systems is a mere consequence of MBPT is at present not so straightforward to address in full generality.

The paper is organized as follows: we start with a description of our model system(s) in Sec. II; then, in Sec. III, we discuss the general properties of the single-particle Green's function; the key ingredient in the KBE. Section IV is an overview of the MBAs used in this work. Section V is devoted to the procedure to obtain the ground state within the KBE. How to solve the KBE for the time evolution is reported in Sec. VI. In Sec. VII, we detail how we extract the TDDFT exchange-correlation potentials corresponding to a chosen MBA. The ground-state and time-dependent results are presented in Secs. VIII and IX, respectively. Section X deals with the correlation-induced damping which occurs during the KBE time evolution and the existence of multiple steady and quasisteady states. Finally, in Sec. XI we present our conclusions and direction for possible future work.

II. MODEL SYSTEMS

We will consider one-dimensional (1D) clusters with M sites and with one orbital at each site. Thus, each site (or, equivalently, each orbital) can accommodate a maximum of

two electrons, with opposite spin. The clusters may either be isolated, in which case the Hamiltonian in standard notation is

$$H_C = -V \sum_{\langle RR' \rangle, \sigma} a_{R\sigma}^\dagger a_{R'\sigma} + U \sum_R \hat{n}_{R\uparrow} \hat{n}_{R\downarrow} + \sum_{R,\sigma} w_R(t) \hat{n}_{R\sigma},$$
(1)

or they may be attached to noninteracting leads of infinite size, as discussed below. In Eq. (1), $\hat{n}_{R\sigma} = a_{R\sigma}^\dagger a_{R\sigma}$, $\sigma = \uparrow, \downarrow$, and $\langle RR' \rangle$ denotes pairs of nearest-neighbor sites. The hopping parameter $V = 1$ and $w_R(t)$ is a local field which includes the time-independent on-site energies as well as the time-dependent external field, which can be of any shape in time t and space. U and $w_R(t)$ are given in units of V. We will consider clusters with $M = 2, 4, 6$ sites and, without leads, $N_e = 2, 6$ electrons (in the presence of leads, the average number of electrons in the clusters is in general noninteger). Our approach is valid for systems which are compensated as well as uncompensated in spin. However, in what follows we will only consider clusters (with/out leads) with an equal average number of spin-up and spin-down electrons in the ground state; this will hold at all times during the dynamics since H has no spin-flip terms. Henceforth, $n = n_\uparrow = n_\downarrow$, where, $n_\sigma = N_\sigma / M$ and $N_\sigma \equiv \langle \sum_{R \in C} \hat{n}_{R\sigma} \rangle$. For both isolated and contacted clusters we refer to the dimensionless quantity, $n_{R\sigma} \equiv \langle \hat{n}_{R\sigma} \rangle$, as the density per spin channel at site R. This convention applies to all figures and discussions in the text.

In the presence of leads, L_α, the Hamiltonian is

$$H = H_C + H_L + H_{LC},$$
(2)

where H_L describes noninteracting one-dimensional semi-infinite chains,

$$H_L = \sum_\alpha \left\{ -V_{L_\alpha} \sum_{\substack{\langle R_\alpha R'_\alpha \rangle, \sigma \\ R_\alpha, R'_\alpha \in L_\alpha}} a_{R_\alpha \sigma}^\dagger a_{R'_\alpha \sigma} + w_{L_\alpha}^B(t) \sum_{\substack{R_\alpha, \sigma \\ R_\alpha \in L_\alpha}} \hat{n}_{R_\alpha \sigma} \right\},$$
(3)

and H_{LC} describes hopping between the central region, C, and the leads

$$H_{LC} = \sum_\alpha \left\{ -V_{L_\alpha C} \sum_{\substack{\langle R_\alpha R' \rangle, \sigma \\ R_\alpha \in L_\alpha, R' \in C}} a_{R_\alpha \sigma}^\dagger a_{R'\sigma} \right\} + \text{H.c.} \quad (4)$$

Here V_{L_α} is the hopping parameter in the αth lead, $w_{L_\alpha}^B$ is the time-dependent bias in such lead and $V_{L_\alpha C}$ is the coupling strength between the lead and the central region.

For isolated clusters, we use a short iterative Lanczos propagation to obtain the exact time evolution. A description of our approach for approximate solutions in isolated and contacted clusters is the object of the next five sections.

III. ONE-PARTICLE GREEN'S FUNCTION

The one-particle Green's function is a reduced quantity, containing much less information than the underlying wave function. In general, it describes a system initially connected
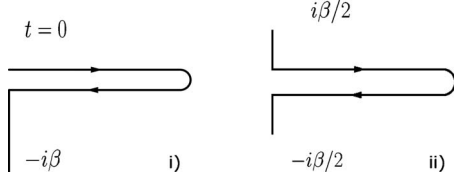
FIG. 1. Keldysh contours.

to a bath with which energy and particle can be exchanged. The knowledge of the Green's function gives access to the expectation values of all single-particle operators, excitation energies, and the total energy of the system.

The general definition of the one-particle Green's function is

$$\mathcal{G}(\mathbf{r}_1\sigma_1 z_1, \mathbf{r}_2\sigma_2 z_2)$$

$$= \langle \mathbf{r}_1\sigma_1 | \hat{\mathcal{G}}(z_1, z_2) | \mathbf{r}_2\sigma_2 \rangle$$

$$\equiv -i \langle \hat{U}(-i\beta, 0) T_\gamma [\hat{\psi}_H(\mathbf{r}_1\sigma_1 z_1)\hat{\psi}_H^\dagger(\mathbf{r}_2\sigma_2 z_2)] \rangle, \quad (5)$$

where $\langle \cdots \rangle$ denotes expectation values of the equilibrium ensemble, $\hat{\psi}_H$ and $\hat{\psi}_H^\dagger$ are the field operators in the Heisenberg picture, γ is the Keldysh contour, see Fig. 1 (i and ii), T_γ is the path ordering operator, $\hat{U}$ is an evolution operator, and $\beta = 1/k_B T$ is the inverse temperature of the bath. The $\mathbf{r}$ and the σ denote the labels corresponding to space (site) and spin coordinates of the adopted single-particle basis. In this basis, the Green's function becomes a matrix. The variable z belongs to the Keldysh contour and is in general complex. For notational convenience, we denote real (imaginary) times by t ($i\tau$). From the definition of the Green's function, one can derive the so-called Kubo-Martin-Schwinger condition,[30] $\mathcal{G}(z_1, z_2) = -\mathcal{G}(z_1, z_2 \pm i\beta)$.

The expectation values of all the single-particle operators are obtained according to

$$\langle A(t) \rangle = -i \operatorname{Tr}[A(t)\mathcal{G}(t, t^+)], \quad (6)$$

where the trace, $\operatorname{Tr} \equiv \Sigma_{r_1 r_2 \sigma\sigma'} \delta_{r_1 r_2} \delta_{\sigma\sigma'}$, is over space and spin indices. As discussed later and in Appendix A, the total energy can be found by evaluating the Galitskii-Migdal (GM) or Luttinger-Ward (LW) functionals.

Since in this paper we study only paramagnetic systems in spin-independent fields, one-particle quantities such as the G and the Σ become spin-diagonal and spin independent,

$$\mathcal{G}(\mathbf{r}_1\sigma_1 z_1, \mathbf{r}_2\sigma_2 z_2) = G(\mathbf{r}_1 z_1, \mathbf{r}_2 z_2)\delta_{\sigma_1\sigma_2}. \quad (7)$$

In the following, we will use the shorthand notation, $1 = (\mathbf{r}_1, z_1)$, etc., for space time coordinates.

The Green's function obeys an integral equation (the so-called Dyson equation),

$$G(12) = G_0(12) + \int_\gamma G_0(13)\Sigma(34)G(42)d34 \quad (8)$$

with the noninteracting Green's function G_0 defined by

$$(i\partial_{z_1} - h(1))G_0(12) = \delta(12). \quad (9)$$

In Eq. (9), h is the noninteracting Hamiltonian.[31] It is convenient to decompose h as $h(t) = \hat{t} + w(t) - \mu$, with (i) $\hat{t}$ the one-particle kinetic energy ($-\nabla_1^2/2$ in coordinate space), (ii) $w(t)$ a local external field which may depend on time, and (iii) μ the chemical potential. The latter is taken to be in between the last occupied and the first nonoccupied level. The inclusion of μ in h implies that the Fermi energy is placed at zero energy; electron/hole excitations thus have positive/negative energies. The kernel of the Dyson equation, Σ, is called the self-energy and is in general nonlocal in space and time. In the exact theory as well as in conserving approximations,[1] the self-energy is a functional of the Green's function, $\Sigma[G]$, and the Dyson equation must thus be solved self-consistently. In equilibrium all quantities depend only on $z = z_2 - z_1$ and the equations are then most easily handled, in terms of Fourier-transformed quantities, in the frequency domain. There, the corresponding Dyson equation becomes a simple matrix equation in the single-particle basis. In this paper, we will work only in the zero-temperature limit in which the system is initially in the ground state. The entire ground-state calculation can be performed using real times and the Dyson equation takes the form

$$G(\epsilon) = G_0(\epsilon) + G_0(\epsilon)\Sigma(\epsilon)G(\epsilon), \quad (10)$$

where ϵ is a real frequency. We alert the reader that using real frequencies is only one of many possible ways of solving the Dyson equation. One advantage of our approach is that we have direct access to the spectral functions.

In equilibrium, all two-point propagators can be expressed in terms of a spectral function. Specializing to the Green's function, the spectral decomposition has the form

$$G(\epsilon) = \int \frac{A(\epsilon')}{\epsilon' - \epsilon + i\eta \operatorname{sgn}(\epsilon')}d\epsilon', \quad (11)$$

where the spectral function, $A(\epsilon)$, is related to the anti-Hermitian part of the corresponding propagator, which for the G is $A(\epsilon) = -\pi^{-1}[G(\epsilon) - G^\dagger(\epsilon)]\operatorname{sgn}(\epsilon)$. The fermionic spectral function are positive definite and the one for G is normalized,

$$\int A(\epsilon)d\epsilon = 1, \quad (12)$$

where 1 represents the identity matrix in the single-particle basis.

IV. MANY-BODY APPROXIMATIONS

In general one cannot construct the exact self-energy and thus needs to rely on approximate schemes. In MBPT, one can systematically construct self-energies of increasing complexity. The main idea is making a diagrammatic expansion of the self-energy, and selecting different classes of diagrams which are then summed up to infinite order. There is a very important group of approximations which conserve quantities such as the total energy, the number of particles, linear and angular momentum, when the system is subject to exter-
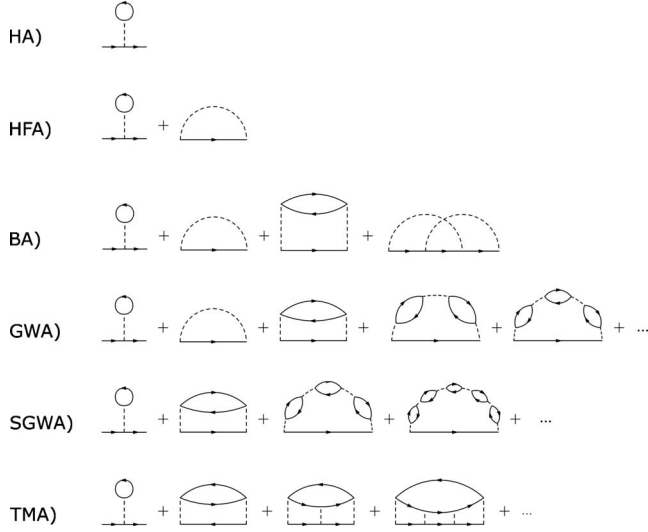
FIG. 2. Diagrammatic expansions of MBAs.

nal fields. These conserving properties are related to the fact that the self-energy is a functional derivative of a generating functional Φ,[1]

$$\Sigma(12) = \frac{\delta \Phi}{\delta G(21)}. \tag{13}$$

The use of conserving approximations is in general very important and, in fact, practically mandatory when studying nonequilibrium phenomena. In general all MBAs are based on partial summations in the sense that they do not take into account all the diagrams of the self-energy. For clarity we distinguish two types of conserving approximations (see Fig. 2), depending on if one includes or not all skeleton diagrams up to a certain order in the interaction strength. The first consists of the Hartree-Fock and the second Born approximations (HFA and BA). The second type contains the Hartree, GW, and T-matrix approximations (HA, GWA, and TMA, respectively).[32] The bare interaction is taken to be local in time, $\mathcal{U}(\mathbf{r_1}, \mathbf{r_2}) \delta(t_1, t_2)$. The formalism we will present is general but we remind the reader that in this paper we will only consider local interactions, $\mathcal{U}(\mathbf{r_1}, \mathbf{r_2}) = U\delta(\mathbf{r_1}, \mathbf{r_2})$ When specialized to our Hubbard clusters with one orbital/site (denoted by R), the on-site interaction can be treated either as spin-dependent, $U\Sigma_R n_{R\uparrow R\downarrow}$ or as spin-independent $\frac{1}{2} U \Sigma_{R\sigma\sigma'} a_{R\sigma}^\dagger a_{R\sigma'}^\dagger a_{R\sigma'} a_{R\sigma}$. These two ways are evidently equivalent in any order by order expansion in skeleton diagrams such as the HFA or the BA. In approximations where not all terms of a given order are included, however, this equivalence may be lost. To illustrate this point, we consider the GWA both spin-independently (GWA) and spin-dependently GWA (SGWA). The TMA is treated only spin dependently.

Hartree-Fock approximation. The simplest many-body treatment is given by the HA, where one takes only the first-order direct term into account (i.e., the exchange is excluded). Due to its rather simple nature, it will not be considered further.

The HFA includes also the first-order exchange diagram and the Fock term. The inclusion of this diagram, among other things, cures the self-interaction of the HA. The resulting self-energy is local in time and thus constant in frequency space. The remaining diagrams are responsible for the many-body correlations and give rise to self-energies which are nonlocal in time.

It is often convenient to separate the time-local HFA and correlation contributions and write

$$\Sigma(z_1, z_2) = \Sigma_{HF} \delta(z_1, z_2) + \Sigma_c(z_1, z_2). \tag{14}$$

Second Born approximation. The simplest scheme which involves correlations is the second Born approximation (BA) which corresponds to keeping all the diagrams up to second order.

GW approximation. The GW approximation is the leading term in the expansion of the self-energy in terms of the dynamically screened interaction W. The expression for the self-energy in time space is given by

$$\Sigma_{GW}(12) = \Sigma_H + iG(12)W(12). \tag{15}$$

It should be noted that this expression does not involve any matrix multiplication. The screening of the bare interaction, U, results from all possible electron-hole excitations which are described by a series of bubble diagrams, involving an irreducible polarization propagator, P. This series can be summed, yielding in frequency space, for a spin-independent interaction,

$$W = \mathcal{U} + \mathcal{U}PW \tag{16}$$

and, for a spin-dependent interaction,

$$\hat{W} = \mathcal{U}P\mathcal{U} + (\mathcal{U}P)^2 \hat{W}. \tag{17}$$

We remind the reader that these Dyson-type equations involve matrix multiplications. In both cases,[33] the polarization propagator, in time space, is

$$P(12) = -iG(12)G(21). \tag{18}$$

T-matrix approximation. The T-matrix approximation comes from building the T-matrix, T, by summing all the ladder diagrams, representing electron-electron or hole-hole scattering.[34] The expression for the self-energy is given by

$$\Sigma_{TM}(12) = \Sigma_{HF} + i \int \mathcal{U}(13)G(43)T(34)\mathcal{U}(42)d34. \tag{19}$$

In the case of an on-site, site-independent interaction this simplifies to

$$\Sigma_{TM}(12) = \Sigma_{HF} + iU^2 G(21)T(12). \tag{20}$$

The sum of the ladder terms in the T-matrix results in

$$T = \phi - \phi \mathcal{U} T, \tag{21}$$

where the so-called irreducible vertex ϕ is defined as

$$\phi(12) = -iG(12)G(12). \tag{22}$$

V. GROUND STATE

The ground state is obtained by solving the Dyson equation, Eq. (10), self-consistently. For clusters contacted to noninteracting leads, the problem can be expressed entirely in terms of propagators which refer only to the central region and an embedding self-energy,[35,36]

$$\Sigma_{emb}(\epsilon) = \sum_{\alpha} |V_{L_{\alpha}C}|^2 \tilde{g}_{L_{\alpha}}(\epsilon), \qquad (23)$$

where $\tilde{g}_{L_{\alpha}}(\epsilon)$ is the noninteracting Green's function of the uncontacted lead L_{α}. The full Green's function in the central region will now obey a Dyson equation with both a many-body and an embedding self-energy. The presence of Σ_{emb} gives rise to continuous spectra, and standard techniques can be used to find self-consistent solutions.

For the isolated clusters, we used a meromorphic representation, as described below.

A. Meromorphic representation of finite systems

For convenience all one-body quantities are represented as matrices in a single-particle basis, e.g., $G_{RR'}(\epsilon) = \langle R|G(\epsilon)|R'\rangle$. In a finite system with a finite phase space, all the spectral functions are discrete,

$$A_{RR'}(\epsilon) = \sum_{j} A_{RR'}^{j} \delta(\epsilon - a_j), \qquad (24)$$

where $A_{RR'}^{j}$ is a residue matrix and a_j is a pole position.

From Eq. (11), we see that the propagators themselves become meromorphic,

$$G_{RR'}(\epsilon) = \sum_{j} \frac{A_{RR'}^{j}}{\epsilon - a_j + i\eta \, \text{sgn}(\epsilon)}. \qquad (25)$$

One main advantage in using a meromorphic representation is that convolutions and cross correlations are made analytically.[37] Given the two functions

$$A_{RR'}(\epsilon) = \sum_{j} \frac{A_{RR'}^{j}}{\epsilon - a_j}, \quad B_{RR'}(\epsilon) = \sum_{j} \frac{B_{RR'}^{j}}{\epsilon - b_j}, \qquad (26)$$

then their cross correlation

$$C_{RR'}(\epsilon) = \int A_{RR'}(\epsilon') B_{RR'}(\epsilon + \epsilon') \frac{d\epsilon'}{2\pi i} \qquad (27)$$

becomes

$$C_{RR'}(\epsilon) = \sum_{jk} A_{RR'}^{k} B_{RR'}^{j} \frac{1}{\epsilon + a_k - b_j}. \qquad (28)$$

A second important attractive feature of a meromorphic representation is that one can compute at once the equilibrium many-body quantities with any time argument, both real and imaginary. For our Hubbard clusters, each of the quantities G, Σ, P, W, ϕ, T will be expressed in such representation during in the actual calculations.

B. Solution to the Dyson equation

The solution to the Dyson equation for the G can formally be written as[38]

$$G(\epsilon) = [G_0^{-1}(\epsilon) - \Sigma(\epsilon)]^{-1} = [\epsilon - h - \Sigma(\epsilon)]^{-1}. \qquad (29)$$

The solution of this matrix equation is obtained in two steps:[37] (1) search of the pole position and (2) calculation of the residue matrix.

(1) The pole positions of G correspond to the zeros of

$$\det[\epsilon - h - \Sigma(\epsilon)], \qquad (30)$$

which we find by ordinary root finding algorithms.

(2) Once the pole positions are found, we calculate the residue matrices by integration in the complex plane. We have in general

$$\oint f(\epsilon) = 2\pi i \sum_{j} \text{Res}(f, a_j), \qquad (31)$$

where

$$f(\epsilon) = \sum \frac{A_j}{\epsilon - a_j}. \qquad (32)$$

If we now perform a closed integration around the pole a_j we obtain directly the residue matrix

$$A_j = \frac{1}{2\pi i} \oint_{a_j} f(\epsilon). \qquad (33)$$

This integration is, in practice, performed numerically.

C. Self-consistency

To reach self-consistency, we start by constructing the self-energy with some initial G, normally taken to be G_0, and then solve the corresponding Dyson equation. The resulting G is then used to build the new self-energy and the procedure is carried on until convergence. In order to keep the number of poles under control (such number increases rapidly from iteration to iteration), we make use of a "decimation" procedure, where poles are merged if there are small or close enough. When two poles are merged, the new pole position is the old center of mass position ("mass" being the trace of the residue matrix) and the new residue matrix is the sum of the two old residue matrices. To improve the convergence we update G by making a linear combination of the new (solution of the Dyson equation) and the old G's. There are different functionals which yield the total energy of a system, all of which are equivalent at the point of stationary solution to the Dyson equation. However, away from self-consistency, they do in general not coincide. One independent way of evaluating the degree of self-consistency is thus by comparing the values of different energy functionals, see Appendix A.

VI. TIME DEPENDENCE

When an external field is applied to a system, the latter is in general driven out of equilibrium. When the system is out of equilibrium and away from the steady-state regime, all the quantities will intrinsically depend on the two time arguments (t_1, t_2) separately and the Keldysh formalism becomes essential. To explicitly show which convention we used in

this paper for the path-ordered two-point Keldysh functions, $\mathcal{K}$, we give some definitions.

A general Keldysh function can be written as

$$\mathcal{K}(12) = \mathcal{K}^\delta(12)\delta(z_1, z_2) + \Theta(12)\mathcal{K}^>(12) + \Theta(21)\mathcal{K}^<(12),$$
(34)

where $>$ ($<$) refers to the electron (hole) part, and $\mathcal{K}^\delta$ the time-local part.

The time coordinates are on the Keldysh contour and may be real or complex. For real times we may also introduce retarded and advanced propagators,

$$\mathcal{K}^R(12) = \mathcal{K}^\delta(12)\delta(z_1, z_2) + \Theta(t_1, t_2)[\mathcal{K}^>(12) - \mathcal{K}^<(12)],$$
(35)

$$\mathcal{K}^A(12) = \mathcal{K}^\delta(12)\delta(z_1, z_2) - \Theta(t_2, t_1)[\mathcal{K}^>(12) - \mathcal{K}^<(12)].$$
(36)

Note that for the $\mathcal{K}$'s considered in the paper, only Σ and W have parts which are local in time.

When both time arguments are imaginary, the Keldysh function reduces to the corresponding equilibrium Matsubara function,

$$\mathcal{K}^M(\tau - \tau') = -i\mathcal{K}(-i\tau, -i\tau').$$
(37)

In Eq. (34), $\Theta(12)$ should be understood as $\Theta(z_1, z_2)$, a generalized Heaviside function for z_1, z_2 on the ordered Keldysh contour. It is worth noting that when both time arguments lie on the imaginary (Matsubara) axis, the quantities represent the initial, equilibrium, state which, as already said, depend only on the time differences. As an example of how these terms are found in equilibrium in the meromorphic representation, we display the hole contribution to the Green's function,

$$G^<(t_1, t_2) = i\sum_{j<\mu} A_j e^{ia_j(t_1 - t_2)}$$
(38)

when both time arguments are real,

$$G^<(t, -i\tau) = i\sum_{j<\mu} A_j e^{ia_j t} e^{a_j \tau}$$
(39)

when both one time argument is real and one imaginary, and

$$G^<(-i\tau_1, -i\tau_2) = i\sum_{j<\mu} A_j e^{-a_j(\tau_1 - \tau_2)}$$
(40)

when both time arguments are imaginary.

A. General symmetries

We recall some prominent symmetry relations which will be used during the time propagation. From the definition of the Green's function, Eq. (5), one can derive a very important symmetry,[39] which enters many relevant and useful relations,

$$G^\gtrless(12) = -G^\gtrless(21)^\dagger.$$
(41)

Additionally, from the definition of the retarded and advanced Green's functions we obtain

$$G^{R/A}(12) = G^{A/R}(21)^\dagger.$$
(42)

From the expansion of the T and W in terms of ϕ and P it follows that T and W will have the same symmetry properties of ϕ and P. The symmetries of ϕ and P can be deduced from their definitions

$$P^\gtrless(12) = -P^\gtrless(21)^\dagger \Rightarrow W^\gtrless(12) = -W^\gtrless(21)^\dagger$$
(43)

and

$$\phi^\gtrless(12) = -\phi^\gtrless(21)^\dagger \Rightarrow T^\gtrless(12) = -T^\gtrless(21)^\dagger.$$
(44)

In a similar way we find a symmetry relation, valid for all approximations, for the self-energy,

$$\Sigma^\gtrless(12) = -\Sigma^\gtrless(21)^\dagger.$$
(45)

An additional symmetry fulfilled by W is

$$W^\gtrless(12) = W^\lessgtr(21),$$
(46)

which implies

$$W^>(z, z) = W^<(z, z), \quad \text{Re } W_{RR'}(z, z) = 0 \quad \forall \ R, R'.$$
(47)

No equivalent relation exists for T.

B. Solving for the nonequilibrium Green's function

To obtain the nonequilibrium Green's function, we need to solve the corresponding equations of motion, called the KBEs,

$$[i\partial_{t_1} - h(1)]G(12) = \delta(12) + \int_\gamma \Sigma(13)G(32)d3,$$
(48)

$$[-i\partial_{t_2} - h(2)]G(12) = \delta(12) + \int_\gamma G(13)\Sigma(32)d3.$$
(49)

The kernel of these equations, the Σ, will in general be a contraction of the Green's function with an other quantity which involves an infinite order summation such as the T or W. These quantities are defined by corresponding integral equations. Specializing to the case of T, we have

$$T(12) = \phi(12) - \int_\gamma \phi(13)\mathcal{U}(34)T(42)d34,$$
(50)

$$T(12) = \phi(12) - \int_\gamma T(13)\mathcal{U}(34)\phi(42)d34.$$
(51)

We thus have two sets of coupled integral equations which need to be solved simultaneously at all times.

C. Solution of coupled integral equations

From the symmetry relations (41), (43), and (44) we see that G and W, T are only needed on the upper/lower time matrix. We choose the lesser components on the upper triangle $t_1 \geq t_2$ and the greater ones on the lower triangle $t_1 < t_2$.[40] Propagation is thus made by expanding the Keldysh
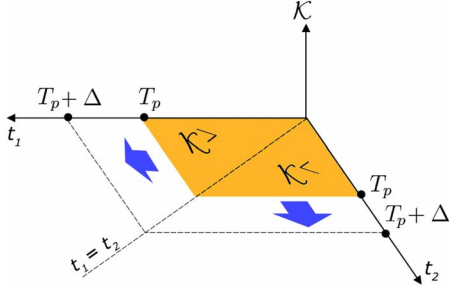
FIG. 3. (Color online) The time-propagation square.

functions, $\mathcal{K}$, on the time square from T_p to $T_p+\Delta$, see Fig. 3. In the integral equations, Eqs. (48)–(51), the function to be determined appears in both the right- and left-hand sides. To solve these equations we use a self-consistent predictor-corrector method.[41] The method can be described schematically by an external loop, where an approximate $\bar{G}$ at T_p $+\Delta$ is generated by propagating Eqs. (48) and (49), and an internal loop, where Eqs. (50) and (51) are solved self-consistently for a fixed kernel $\phi[\bar{G}]$ or $P[\bar{G}]$. The external loop is performed by a predictor-corrector method described below while the internal one is solved by the same iteration method as described for the ground state. The external loop is initiated by an extrapolated value of the collision integrals $\int_\gamma \Sigma_c G$, while the internal loop is started by an extrapolated value of the W, T. The new time step is generated when the external loop achieves self-consistency.

D. Kadanoff-Baym equations

When propagating the Green's functions it is convenient to separate the terms which are local in time and single-particlelike (h and Σ_{HF}) from the remaining correlation-induced ones[41] and introduce

$$\mathfrak{h} = h + \Sigma_{HF}. \tag{52}$$

In this way, $\mathfrak{h}$ replaces h and the full self-energy is replaced by its correlation part Σ_c in the KBE [cf. Eqs. (48) and (49)]. The reason for this partitioning is twofold: on the one hand the contribution from the single-particle evolution is very important (and could thus lead to large numerical errors in the correlation contribution) and on the other it can be solved essentially in an exact way as will be detailed in Sec. VI E.

There are several equivalent contours on which one can define the KBE. We use the contour (ii) in Fig. 1, which is numerically more stable and has an analytical limit when the temperature goes to zero. The reason is that due to the Kubo-Martin-Schwinger condition the Green's function will in contour (i) be large around zero and at $-\mathrm{i}\beta$ (which must therefore be finite) and thus one needs dense mesh points at two different regions.[42] The contour (ii), on the other hand, needs dense mesh points only around 0 and the limit $\beta\to\infty$ can be taken without any numerical difficulty.

Once we specialize to this contour, the KBE become

$$i\partial_{t_1} G^{\lessgtr}(t_1, t_2) = \mathfrak{h}(t_1) G^{\lessgtr}(t_1, t_2) + I_1^{\lessgtr}(t_1, t_2), \tag{53}$$

$$-i\partial_{t_2} G^{\lessgtr}(t_1, t_2) = G^{\lessgtr}(t_1, t_2)\mathfrak{h}(t_2) + I_2^{\lessgtr}(t_1, t_2), \tag{54}$$

$$i\partial_t G^<(t, -i\tau) = \mathfrak{h}(t) G^<(t, -i\tau) + I^<(t, -i\tau), \tag{55}$$

$$-i\partial_t G^>(-i\tau, t) = G^>(-i\tau, t)\mathfrak{h}(t) + I^>(-i\tau, t), \tag{56}$$

where the collision integrals with both time arguments real are

$$I_1^{\lessgtr}(t_1, t_2) = \int_0^{t_1} d\bar{t}[\Sigma_c^R(t_1, \bar{t})G^{\lessgtr}(\bar{t}, t_2) + \Sigma_c^{\lessgtr}(t_1, \bar{t})G^A(\bar{t}, t_2)]$$
$$+ \frac{1}{i}\int_0^{\beta/2} d\bar{\tau}[\Sigma_c^<(t_1, -i\bar{\tau})G^>(-i\bar{\tau}, t_2)$$
$$+ \Sigma_c^>(t_1, i\bar{\tau})G^<(i\bar{\tau}, t_2)], \tag{57}$$

$$I_2^{\lessgtr}(t_1, t_2) = \int_0^{t_2} d\bar{t}[G^R(t_1, \bar{t})\Sigma_c^{\lessgtr}(\bar{t}, t_2) + G^{\lessgtr}(t_1, \bar{t})\Sigma_c^A(\bar{t}, t_2)]$$
$$+ \frac{1}{i}\int_0^{\beta/2} d\bar{\tau}[G^<(t_1, -i\bar{\tau})\Sigma_c^>(-i\bar{\tau}, t_2)$$
$$+ G^>(t_1, i\bar{\tau})\Sigma_c^<(i\bar{\tau}, t_2)]. \tag{58}$$

The collision integrals with one of the time arguments complex specialize to

$$I^<(t, -i\tau) = \int_0^t d\bar{t}\Sigma_c^R(t, \bar{t})G^<(\bar{t}, -i\tau)$$
$$+ \int_0^{\beta/2} d\bar{\tau}[\Sigma_c^<(t, -i\bar{\tau})G^M(\bar{\tau} - \tau)$$
$$+ \Sigma_c^>(t, i\bar{\tau})G^M(-(\bar{\tau} + \tau))], \tag{59}$$

$$I^>(-i\tau, t) = \int_0^t d\bar{t}G^>(-i\tau, \bar{t})\Sigma_c^A(\bar{t}, t)$$
$$+ \int_0^{\beta/2} d\bar{\tau}[G^M(\tau - \bar{\tau})\Sigma_c^>(-i\bar{\tau}, t)$$
$$+ G^M(\tau + \bar{\tau})\Sigma_c^<(i\bar{\tau}, t)]. \tag{60}$$

It is worth noting that all Eqs. (57)–(59) contain terms which involve integration along the Matsubara (vertical) axis and which represent the memory of the initial state correlations during the time evolution.

For the collision integrals, one can derive a similar symmetry property,

$$I_1^{\lessgtr}(12) = -I_2^{\lessgtr}(21)^\dagger. \tag{61}$$

An important consequence of this relation is that the densities[43] are manifestly real. From the KBE one can derive that the condition for real densities is given by

$$[I_1^<(t, t) - I_2^<(t, t)] = [I_1^<(t, t) - I_2^<(t, t)]^\dagger, \tag{62}$$

which is manifestly satisfied by Eq. (61). Furthermore, on the time diagonal, we obtain another relation, which is very useful in from the computationally point of view,

$$I^{\lessgtr}_{1/2} = I^{\gtrless}_{1/2}. \tag{63}$$

From the properties of integral equations, it follows that all the symmetry and structure properties of the Green's function are those of G_0.

The discussion of the KBE above is valid for extended and finite systems alike. When the interaction is confined to a central region which is contacted to possibly macroscopic leads, the problem can again be expressed in propagators which refer only to the central region, and an embedding self-energy which now depends on time,[13,14]

$$\Sigma_{emb}(t_1,t_2) = \sum_\alpha |V_{L_\alpha C}|^2 \widetilde{g}_{L_\alpha}(t_1,t_2). \tag{64}$$

Here $\widetilde{g}_{L_\alpha}(t_1,t_2)$ is the noninteracting Green's function of the uncontacted lead L_α, possibly subject to a uniform but time-dependent bias. The full Green's function in the central region will now obey the KBE with both the self-energy from the interaction and the one from the leads via the embedding. The embedding self-energy is entirely nonlocal in time and will be treated on the same footing as the correlation part of the interaction self-energy. It is worth noting that the embedding self-energy involve no self-consistency and can thus be calculated once the external bias (if present) is known.

E. Time propagation algorithm

As mentioned in Sec. VI D, we treat the time-local part of the self-energy (Σ_{HF}) on the same footing as the noninteracting terms (h) in the time propagation, by defining $\mathfrak{h} = h + \Sigma_{HF}$. The evolution from these single-particle terms can be expressed in terms of a single-particle evolution operator S which is a time-dependent matrix in single-particle labels.[41] This leads to the following unitary gauge transformation:

$$G^{\lessgtr}(t_1,t_2) = S(t_1,0)g^{\lessgtr}(t_1,t_2)S^\dagger(t_2,0), \tag{65}$$

where S satisfies $i\partial_{t_1}S(t_1,0) = \mathfrak{h}(t_1)S(t_1,0)$. The expression for $G^>$ at time $T_p + \Delta$ becomes

$$\begin{aligned} G^>(T_p + \Delta, t_2) = {} & S(T_p + \Delta, T_p)G^>(T_p,t_2) \\ & - iS(T_p + \Delta, T_p) \\ & \times \int_0^\Delta d\bar{t}\, S^\dagger(\bar{t} + T_p, T_p)I_1^>(\bar{t} + T_p, t_2). \end{aligned} \tag{66}$$

Similar expressions exist for the other Green's functions. For full a derivation, see Appendix B.

F. Dyson equation for T and W

Propagating in time the KBE within a specific MBA-based partial summation, requires solving a Dyson equation for auxiliary quantities which enter the expression for the self-energy.[44] For the TMA and GWA such quantities are the T and W, respectively. The components of the corresponding Dyson equations (again specialized to the case of T) Eqs. (50) and (51) are, for both times on the real axis,

$$\begin{aligned} T^{\lessgtr}(t_1,t_2) = {} & \phi^{\lessgtr}(t_1,t_2) \\ & - \int_0^{t_1} d\bar{t}[\phi^R(t_1,\bar{t})\mathcal{U}T^{\lessgtr}(\bar{t},t_2) + \phi^{\lessgtr}(t_1,\bar{t})\mathcal{U}T^A(\bar{t},t_2)] \\ & - \frac{1}{i}\int_0^{\beta/2} d\bar{\tau}[\phi^<(t_1,-i\bar{\tau})\mathcal{U}T^>(-i\bar{\tau},t_2) \\ & + \phi^>(t_1,i\bar{\tau})\mathcal{U}T^<(i\bar{\tau},t_2)], \end{aligned} \tag{67}$$

$$\begin{aligned} T^{\lessgtr}(t_1,t_2) = {} & \phi^{\lessgtr}(t_1,t_2) \\ & - \int_0^{t_2} d\bar{t}[T^R(t_1,\bar{t})\mathcal{U}\phi^{\lessgtr}(\bar{t},t_2) + T^{\lessgtr}(t_1,\bar{t})\mathcal{U}\phi^A(\bar{t},t_2)] \\ & - \frac{1}{i}\int_0^{\beta/2} d\bar{\tau}[T^<(t_1,-i\bar{\tau})\mathcal{U}\phi^>(-i\bar{\tau},t_2) \\ & + T^>(t_1,i\bar{\tau})\mathcal{U}\phi^<(i\bar{\tau},t_2)], \end{aligned} \tag{68}$$

when one of the time arguments is imaginary we have

$$\begin{aligned} T^<(t,-i\tau) = {} & \phi^<(t,-i\tau) - \int_0^t d\bar{t}\phi^R(t,\bar{t})\mathcal{U}T^<(\bar{t},-i\tau) \\ & - \int_0^{\beta/2} d\bar{\tau}[\phi^<(t,-i\bar{\tau})\mathcal{U}T^M(\bar{\tau}-\tau) \\ & + \phi^>(t,i\bar{\tau})\mathcal{U}T^M(-(\bar{\tau}+\tau))], \end{aligned} \tag{69}$$

$$\begin{aligned} T^>(-i\tau,t) = {} & \phi^>(-i\tau,t) - \int_0^t d\bar{t}T^>(-i\tau,\bar{t})\mathcal{U}\phi^A(\bar{t},t) \\ & - \int_0^{\beta/2} d\bar{\tau}[T^M(\tau-\bar{\tau})\mathcal{U}\phi^>(-i\bar{\tau},t) \\ & + T^M(\tau+\bar{\tau})\mathcal{U}\phi^<(i\bar{\tau},t)]. \end{aligned} \tag{70}$$

VII. TDDFT EXCHANGE-CORRELATION POTENTIAL FROM MBPT

Our time-dependent densities from the different MBAs also provide insight for the TDDFT exchange-correlation potentials for strongly correlated systems. Given a specific approximation, from the resulting time-dependent density we obtain the corresponding effective potential $v_{eff} = \Sigma_H + w + v_{xc}$, where Σ_H is the Hartree potential and v_{xc} the exchange correlation potential. In practice, this is done via a numerical reverse engineering procedure.[29] This algorithm imposes that $|n(R,t) - n^{KS}(R,t)| = 0$ at each time step, where $n^{KS}(R,t) = \Sigma_\nu^{occ}|\psi_\nu^{KS}(R,t)|^2$ is the Kohn-Sham density and ψ_ν^{KS} are the Kohn-Sham orbitals. The n^{KS} is found by solving $i\dot{\psi}_\nu^{KS} = (\hat{t} + v_{eff})\psi_\nu^{KS}$ where the kinetic energy is given by $\hat{t} = -V\Sigma_{\langle RR'\rangle\sigma}a_{R\sigma}^\dagger a_{R'\sigma}$.

VIII. RESULTS: GROUND STATE

To start the time propagation of the KBE, one needs the initial, equilibrium, one-particle propagators. These are
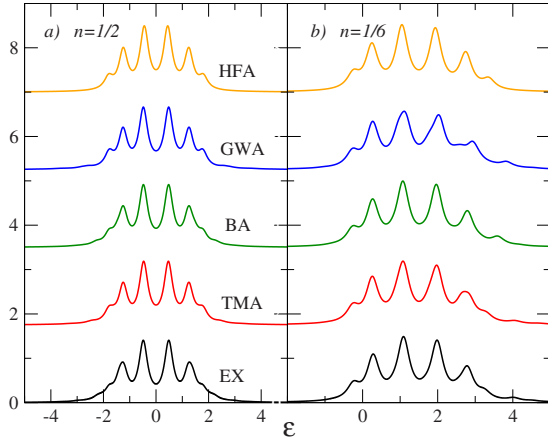
FIG. 4. (Color online) Ground-state spectral functions for $M=6$ for weak interaction strength, $U=1$, for different fillings. The curves correspond to exact (black), TMA (red), BA (green), GWA (blue), and HFA (orange). The curves are shifted for clearer comparison and we have broadened the discrete spectra with a Lorentzian with a FWHM=0.4. The frequency is given in units of the hopping parameter of the central region, V.

found by solving the Dyson equation self-consistently. Here, we show only results for isolated clusters, and defer the case of clusters contacted to leads to Sec. X.

To characterize the ground-state properties, we present in Figs. 4–6 the spectral functions at the first, $R=1$, site in the cluster. This is the site at which the external perturbation is applied (see Sec. IX). In the following, if not stated otherwise, the on-site energies in Eq. (1) are put to zero. The results we will show are for the different MBAs, at two particle concentrations and interaction strengths. A first, general comment is that the performance of the MBAs generally worsens with increasing U. Some basic, generic features of the different MBAs we employ to evolve in time our clusters are already revealed by the ground-state results. Such fea-
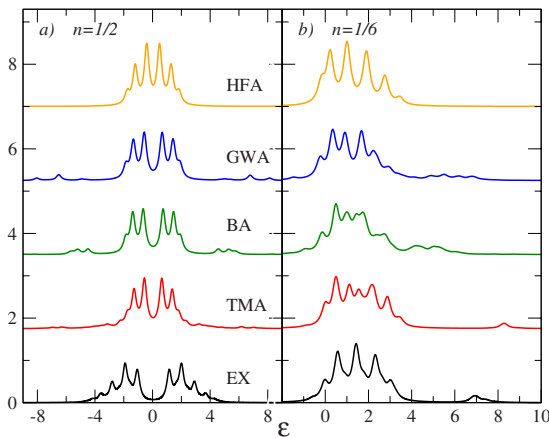
FIG. 5. (Color online) Ground-state spectral functions for $M=6$ for strong interaction strength, $U=4$, at different fillings. The curves correspond to exact (black), TMA (red), BA (green), GWA (blue), and HFA (orange). The curves are shifted for clearer comparison and we have broadened the discrete spectra with a Lorentzian with a FWHM=0.4. The frequency is given in units of the hopping parameter of the central region, V.
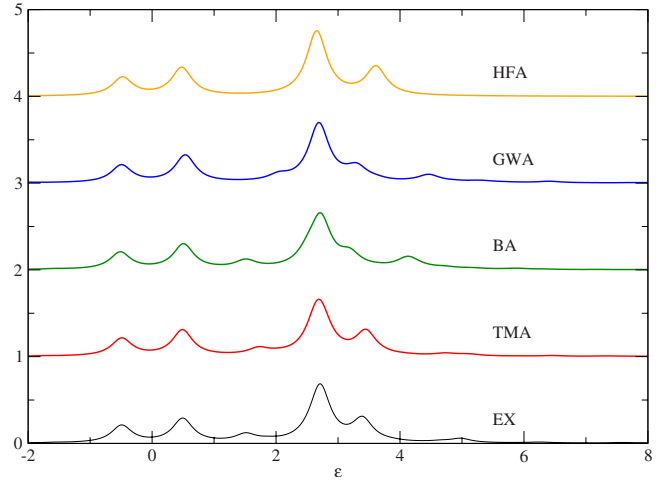
FIG. 6. (Color online) Ground-state spectral functions for $M=6$ ordered as a ring at $n=1/6$ for $U=2$. The on-site energies vary periodically between 0 and -1, starting with 0 on site 1. The curves correspond to exact (black), TMA (red), BA (green), GWA (blue), and HFA (orange). The curves are shifted for clearer comparison and we have broadened the discrete spectra with a Lorentzian with a FWHM=0.4. The frequency is given in units of the hopping parameter of the central region, V.

tures, specifically discussed for the cases in Figs. 4 and 5, are common to other clusters with different fillings, sizes, and interactions strengths (such additional results are not shown). Figure 4 refers to the situation of weak interaction, where the performance of the MBAs is satisfactory (in particular, all the MBAs reproduce the symmetry breaking at low filling of the exact solution).

At half filling, a correlation gap opens on increasing U, which becomes clearly visible in the strong correlation regime, Fig. 5. This behavior in clusters is consistent with the exact solution of the one-dimensional (1D) Hubbard model in the thermodynamical limit.[45] This feature is reproduced by the different approximate schemes. However, the size of the approximate gap depends on the MBA: the best estimate is given by the BA value; yet, the latter largely underestimates the exact value. Missing the contribution of correlation effects, the nonmagnetic HFA solutions reproduce the noninteracting spectral density. As a second general feature, the MBAs introduce spurious satellites away from the band region. This problem is most pronounced in the BA and GWA curves. In the low-density regime, for large U, a satellite structure appears in the exact solution [about 6.5 in the bottom of panel 4(b)]. In an extended system, this high-energy spectral feature represents a two-electron antibound state (i.e., outside the band continuum). The satellite is well reproduced by the TMA (although its distance from the band region is overestimated) while is smeared out in the BA and GWA and obviously absent in the HFA (as it includes no correlation effects). For the strong interaction case, the agreement of the different approximations with the exact curve in the band region is only moderate.

Similar conclusions can be drawn for different geometries. For example, in Fig. 6 we plot the spectral function of a six-site ring cluster, i.e., with periodic boundary conditions,
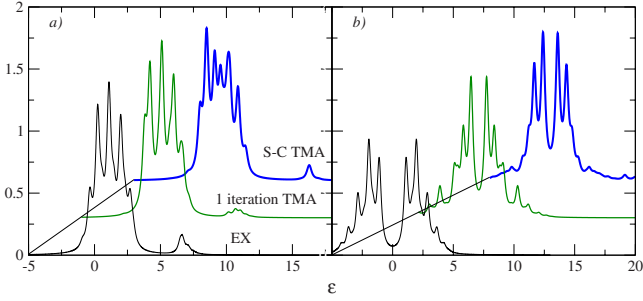
FIG. 7. (Color online) First-iteration TMA, and self-consistent TMA spectral function versus the exact one. $M=6$ and in (a) $n =1/6$ and in (b) $n=1/2$. The curves correspond to exact (black), first iteration TMA (green), and self-consistent TMA (thick blue). The curves are shifted for clearer comparison and we have broadened the discrete spectra with a Lorentzian with a FWHM=0.4. The frequency is given in units of the hopping parameter of the central region, V.

where the on-site energies vary periodically between 0 and −1 starting with 0 at the first site. In this case we see that the TMA is substantially better than the BA and the GWA, especially at higher frequencies. The HFA reproduces the main central peaks quite accurately but misses the structure at high frequencies.

In all our results, when comparing the SGWA to the GWA we see a slight improvement, which is expected, as the SGWA includes fewer faulty diagrams. This improved version of the GWA is, however, still worse than the BA or the TMA. In this section, we show no results for the SGWA since it introduces only a marginal improvement in the ground-state spectral density: however, we will present below SGWA time-dependent densities. It is worth noticing that, using a MBA expansion in terms of nonmagnetic propagators, the SGWA will have a magnetic instability on increasing U. This can be seen most easily in a Hubbard dimer with two electrons with opposite spins. In the dimer, where the poles of $W[G_0]$ are $\epsilon= \pm \sqrt{4V^2 \pm 2VU}$, this unphysical symmetry breaking occurs for $U \geq 2V$. Conversely, the exact ground state for a dimer is always a spin $S=0$ (singlet) state, since, for any positive U, the dimer ground-state energy $E_{gs}^{dimer}=E_{dimer}^{S=0}=\frac{U-\sqrt{16V^2+U^2}}{2}<0=E_{dimer}^{S=1}$.

It is worth noting that all the spectral functions shown in Figs. 4 and 5 are not as good as those obtained without self-consistency, i.e., when stopping after the first iteration of the Dyson equation, see Fig. 7. This is an example of the known fact that self-consistent conserving approximations often have worse spectral properties than nonself-consistent ones.[37,46,47] To guarantee the fulfillment of the conservation laws and to get unambiguous total-energy results, it is capital to achieve self-consistency. If the quantity of interest is the spectral functions one should instead make use of different partial summation criteria,[46] and in some cases include vertex corrections to remove artifacts introduced by self-consistency.[37]

As a final remark to this section, we note that all MBAs which have a frequency-dependent self-energy involve infinitely many possible excitations. These excitations, represented by diagrams in the self-energy, result in infinitely

many, but discrete, number of poles in the ground-state spectral functions.[48] The exact solution, in contrast, lives in a finite phase space which implies a finite number of poles. The poles of these MBAs are typically distributed with some few large and well-isolated poles with the largest part of the oscillator strength and many small ones which get closer and closer out in the tails. This can be seen in Fig. 8, where we plot the (artificially) broadened and the unbroadened spectral functions, for a specific case. The general remarks made about Fig. 8 apply to all the cases we have studied.

FIG. 8. (Color online) Broadened (black) and unbroadened (red) spectral function in the TMA for $M=4$, $n=1/2$, and $U=2$. The broadening of the discrete spectra is done with a Lorentzian with a FWHM=0.4. The unbroadened spectral function has been scaled with a factor of 1.65 to adjust the height of the central peaks to those of the broadened one. The frequency is given in units of the hopping parameter of the central region, V.

IX. RESULTS: TIME DEPENDENCE

In this section, we examine the performance in time of the different MBAs. To accomplish this, we use as benchmark exact many-body solutions. In general, the latter are available only for finite systems, and numerical in nature. As a consequence, in this section we deal exclusively with isolated clusters, and focus on general aspects of the time-dependent densities and MBAs. However, we defer to the next section two important outcomes of the KBE time evolution: the correlation-induced damping and the existence of multiple steady states in isolated and contacted clusters. Since these features appear in the long-time behavior, here we focus on short time response.

Isolated clusters: MBAs vs exact results. We start the time evolution at $t=0$ with the ground-state Green's function. For positive times $t>0$ we apply a spin-independent external field to the system. We have studied different types of external fields but in this paper we present results only for the form $w_R(t)=w_0 \delta_{R,1} \Theta(t)$, i.e., we consider a step perturbation and let it to act only on the leftmost, $R=1$, site. The time is given in units of the inverse hopping parameter $(1/V)$ and all curves represent the dynamics on site $R=1$. The cases displayed are the same as those considered for the ground-state results.
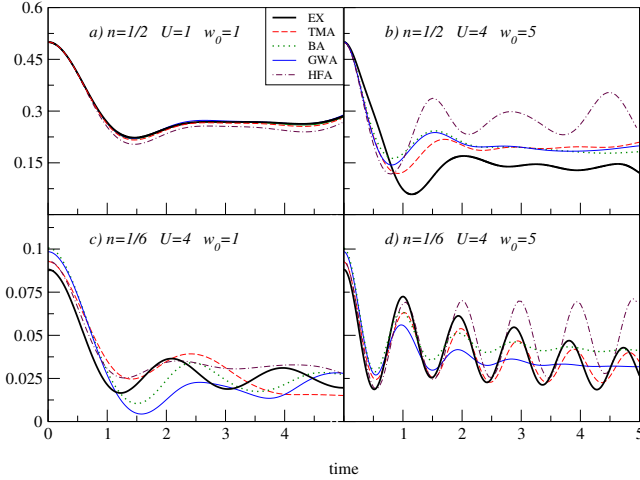
FIG. 9. (Color online) Time-dependent densities on site 1 for $M=6$. The curves correspond to exact (thick solid black), TMA (dashed red), BA (dotted green), GWA (thin solid blue), and HFA (brown dashed dot). The time is given in units of the inverse hopping parameter of the central region, V^{-1}.

FIG. 10. (Color online) Time-dependent densities on site 1 for a ring-shaped cluster with $M=6$ sites and filling $n=1/6$, for $U=2$ and $w_0=5$. The on-site energies vary periodically between 0 and -1, starting with 0 on site 1. The curves correspond to exact (thick solid black), TMA (dashed red), BA (dotted green), GWA (thin solid blue), and HFA (brown dashed dot). The time is given in units of the inverse hopping parameter of the central region, V^{-1}.

We show the resulting time-dependent densities in Fig. 9. The curves correspond to some initial states shown in Figs. 4 and 5. In the panels (a) and (b), $n=1/2$ while in panels (c) and (d), $n=1/6$. In the simplest case ($U=1$, $w_0=1$), presented in panel (a), all MBAs give a good description of the density. On increasing the strength of the interaction and the external field, panel (b), we clearly see that the HFA description is rather crude while the curves from the other MBAs are very similar to each other and closer to the exact density. In the case of strong interaction but weak field, panel (c), we see that none of the MBAs give an adequate description. We interpret these results as a consequence to the fact that the ground-state spectral function is not well described in the band region: the latter is responsible for the response to weak fields. On the contrary, for low filling and when the field is strong, panel (d), the TMA performs much better than the other MBAs. This is due to the fact that the nonlinear response involves states at higher excitation energy and the TMA is the only approximation which, to some extent, reproduces the satellite structure.

The TMA stands out as the best approximation at low filling also for other geometries. In Fig. 10, we see the time-dependent densities for the ring geometry where the BA and GWA perform much worse than both the HFA and the TMA.

It is useful at this point to mention that when analyzing the nonequilibrium performance of the different MBAs in terms of ground-state properties we refer to the intrinsic properties of the MBAs and not on the initial state. In fact we will in Sec. X see that the propagation is insensitive to the initial state.

Isolated clusters: MBAs, exact results and TDDFT. It is interesting to examine some of the results just presented from a TDDFT perspective. A clear advantage of TDDFT is that, for the time evolution, it deals with quantities with a single time argument (one is propagating the Kohn-Sham orbitals). Nevertheless, a key requirement in TDDFT is that v_{xc} (an thus v_{eff}) should depend in a nonlocal (in space and
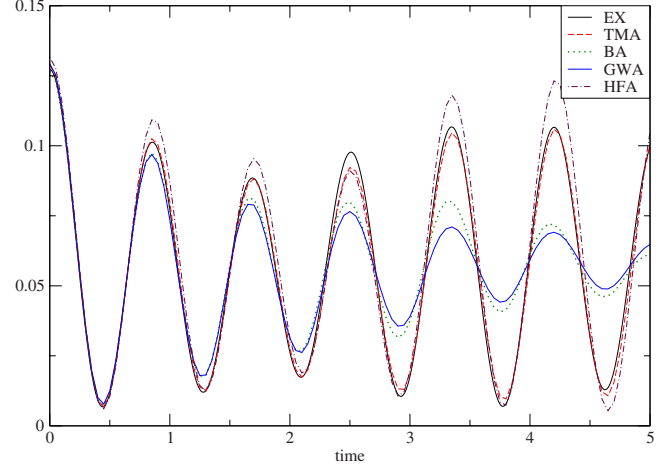
time) fashion on the particle density. In this way, all the complexities of the many-body dynamics are subsumed into a highly nontrivial dependence of v_{xc} on the density. Not surprisingly, making progress in the construction of improved XC functional is a rather challenging task, especially for strongly correlated systems. It is also true that, in some cases, simple adiabatic local approximations can provide satisfactory results; this is also the case for a TDDFT description of the Hubbard model in nonequilibrium.[29,49] However, memory and nonlocal effects should in general be taken into account. The so-called variational approach to TDDFT,[50,51] has the advantage of a systematic inclusion of many-body contributions in the XC potential. Also, in this way nonlocality in space and memory effects are properly included, once v_{xc} is retrieved from the many-body self-energy via the time-dependent Sham-Schlüter equation.[52] Deferring a "bottom-up" construction of v_{xc} via MBAs to future work, we here still wish to explore the connection between TDDFT and MBAs on the Keldysh contour, looking at exchange-correlation potentials obtained via time-dependent reverse engineering using the time-dependent densities from the KBE. The results of this procedure are presented in Fig. 11, $M=6$, $N=2$, $U=4$, $w_0=5$. This corresponds to the time-dependent densities presented in panel (d) of Fig. 9. Consistently with the density results, we see the v_{eff} in the TMA is superior to those from the other MBAs, and quite close to the exact one. We also note the large discrepancy of the HFA and that, for both the BA and the GWA, v_{eff} exhibits a damped behavior [the same is observed in the densities in panel (d) of Fig. 9, see Sec. X below). In spite of not being perfect, the agreement of v_{eff} from the TMA with the exact one is quite encouraging, suggesting that there is ample scope for pursuing the construction of improved v_{xc} from (suitably chosen) MBAs.

Spin-dependent GWA. Before concluding this section, we wish to discuss briefly the effect on making a spin-dependent
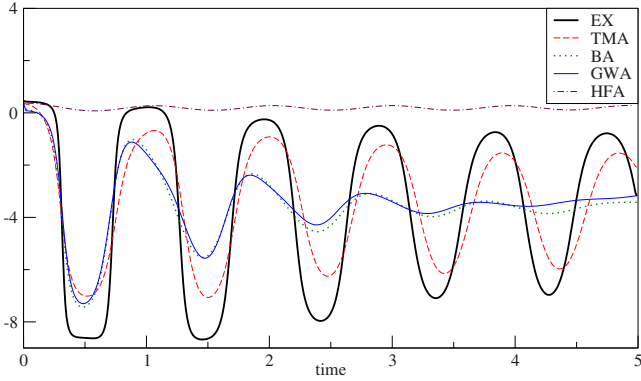
FIG. 11. (Color online) Time-dependent v_{eff} on site 1 for M =6, U=4, and w_0=5. The curves correspond to exact (thick solid black), TMA (dashed red), BA (dotted green), GWA (thin solid blue), and HFA (brown dashed dot). The time is given in units of the inverse hopping parameter of the central region, V^{-1}.

treatment in the GWA. In Fig. 12, we make a comparison between GWA, SGWA, and, for reference, TMA. Due to the symmetry breaking of the SGWA (see Sec. VIII), and that we only consider the spin unpolarized case (otherwise, one should start with polarized propagators) we confine ourselves to the weak interaction regime. As evident from Fig. 12, for the chosen parameters the SGWA is slightly better than its spin-independent counterpart but inferior to the TMA.

As a final remark to this section, we note that in the general case, GWA was designed to give a good screening of the Coulomb interaction,[21] which in our system has already been taken into account indirectly by the model itself. The TMA, on the other hand, is known to give a good performance if the interaction is short ranged, especially in the low-density regime.[22] The general good description of the TMA (both in and out of equilibrium) for the short-ranged Hubbard Hamiltonian is in accordance to previous studies of ground-state properties of clusters.[37,53] Both ground-state and time-
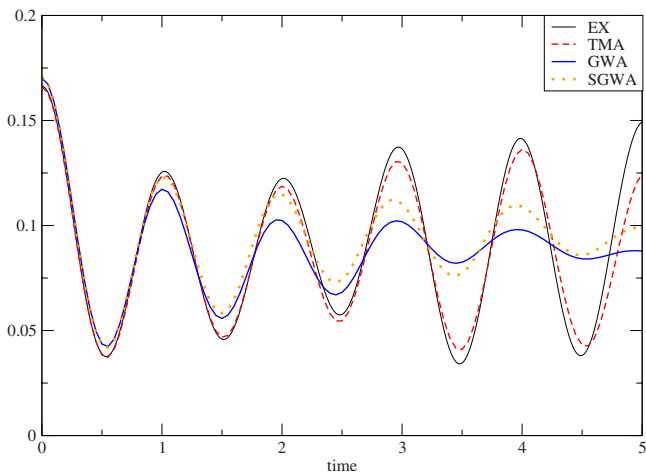
FIG. 12. (Color online) Time-dependent densities for M =4, U=1.5, w_0=5 and n=1/4. The curves correspond to exact (black), GWA (dotted red), SGWA (thick blue), and TMA (dashed green). The time is given in units of the inverse hopping parameter of the central region, V^{-1}.
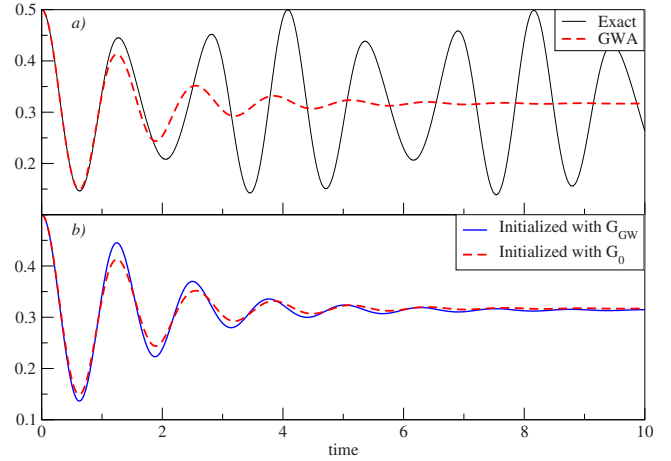
FIG. 13. (Color online) Densities for M=2, n=1/2, U =1, w_0=5, exact (black), GWA (dashed red), and GWA initialized with G_0 (blue). In (a): damping of GWA density versus exact solution. In (b): time-dependent densities for the GWA, initialized with the self-consistent GWA ground state and the noninteracting G_0. The time is given in units of the inverse hopping parameter of the central region, V^{-1}.

dependent results reflect intrinsic properties of an MBA. Moreover, we find here that the performance of the different MBAs in the ground state correlates strongly with their behavior out of equilibrium. In particular, MBAs which give a good description of satellites and band gaps in the ground state are those which perform best in the presence of time-dependent fields.

X. RESULTS: DAMPING AND MULTIPLE STEADY STATES

In this section, we will investigate the correlation-induced damping and the long-time behavior of the KBE. We find that these features are general for all MBAs which include correlation effects. We exemplify this by presenting results for different MBAs in the various parts of this section.

A. Isolated clusters: correlation-induced damping and multiple steady states

Numerical evidence of correlation-induced damping. When we let our isolated system(s) evolve under the action of a strong $(w_0 \gg V)$ external field we reach an artificial steady state,[17,54] see Fig. 13(a). The damping mechanism behind such behavior is not a mere consequence of the infinite number of poles in the initial state but is rather intrinsically linked to the time propagation scheme. To show this fact we present in Fig. 13(b) the time-evolved density initiated with the noninteracting propagator G_0,[55] which has a finite number of poles. From the curves in Fig. 13(b) it is evident that the noninteracting initial state leads to a very similar damped density profile. Note that the similarity of the curves in Fig. 13(b), indicate a robustness of the KBE time evolution against the initial conditions.

The damping is not a numerical artifact: in Fig. 14 we see that particle and energy conservation are strictly obeyed
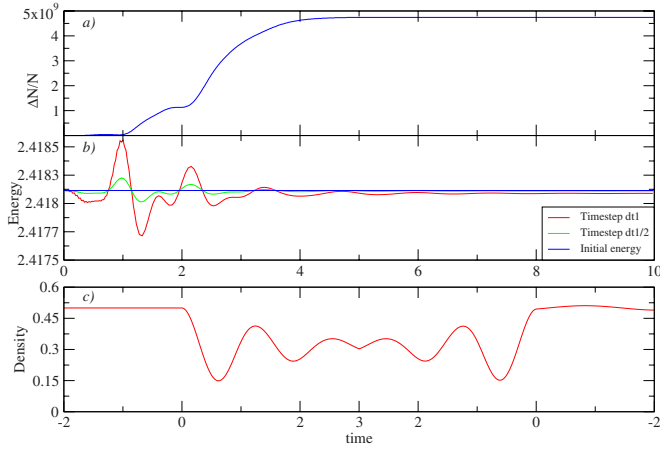
FIG. 14. (Color online) Conservation laws and time reversal in the GWA for $M=2$, $n=1/2$, $U=1$, $w_0=5$. In (a): relative change in particle number. In (b): total energy for different time steps. In (c): density propagated forward in time from -2 to 3 and then backward from 3 to -2. The time is given in units of the inverse hopping parameter of the central region, V^{-1}.

FIG. 15. (Color online) Time-dependent spectral functions in the GWA for $M=2$, $n=1/2$, $U=1$, $w_0=2$, (a): in energy space and (b): in time space. The different curves correspond to $T_p=10$ (black), $T_p=35$ (red), and $T_p=100$ (blue). The time is given in units of the inverse hopping parameter of the central region, V^{-1}.

within our numerical accuracy, see top and middle panel. Moreover, the evolution satisfies time-reversal symmetry. That is, when we reverse the direction of time in the propagation, the system goes back to the initial state and remains there, see bottom panel. The damping rate increases with the strength of the external field and is absent in the regime of linear response.

To study the nonlinear response regime, we find convenient to introduce the instantaneous spectral function,

$$A(T_p,\omega) = -\operatorname{Tr}\operatorname{Im}\int_{-2T_p}^{2T_p} e^{i\omega\tau}[G^> - G^<]\left(T_p+\frac{\tau}{2},T_p-\frac{\tau}{2}\right)d\tau,$$
(71)

where $T_p=(t_1+t_2)/2$ and $\tau=(t_1-t_2)$, and its counterpart in time space. When reaching the steady state, the spectral function gets broadened in energy space, Fig. 15(a), and damped in time space, Fig. 15(b). Note that, for our dimer, the exact instantaneous spectral function would continue to oscillate in time space. The different MBAs have different damping rates; among them, the TMA is in general the slowest. The damping acts strongest on the perturbed site, it generally decreases with system size and is most important at half filling.

Perturbation strength and damping. We have seen, from our numerical results that the correlation damping is absent in the linear regime. The dynamics in this limit is described by the Bethe-Salpeter equation, with a kernel $\delta\Sigma/\delta G$. The latter would have a discrete spectrum in our MBAs, and so would the resulting density response. A discrete response function will in turn lead to a nondamped dynamics. We wish to stress that in a formulation based on conserving MBAs, the key quantity is the generating functional; the corresponding G is then defined via the self-consistent KBE, and not via an underlying wave-function scheme. Without the connection to the underlying wave function, there is no guarantee that, for example, systems with a finite phase space will only
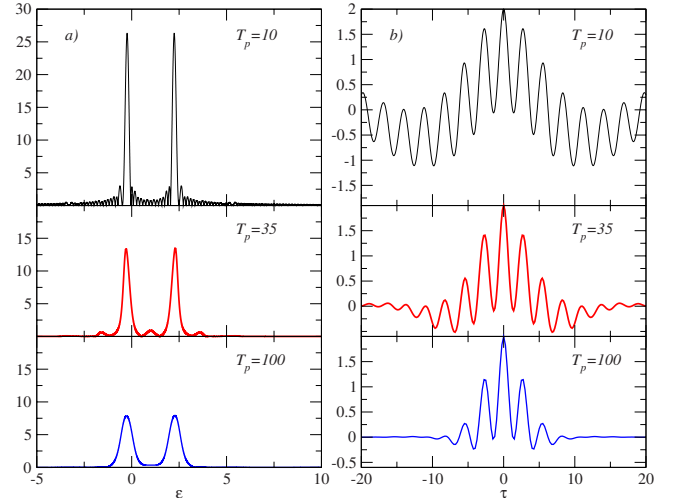
have a finite number of excited states or that they will not have a damped dynamics.

System size and damping. In our study, we have not made an exhaustive characterization of how the large-size limit is gradually obtained; this is indeed an issue we plan to address in future work. Still, we wish to present in the rest of this section some general considerations on the effect of system size on the damping behavior.

In an exact treatment, a finite system has a corresponding finite phase space and will thus not be able to fully relax to a stationary steady state. In a large but finite phase space it will, due to decoherence, give rise to a pseudosteady state but with some long-time revivals. The larger the system gets, the more and more complete the damping becomes. Thus, after a long time, in an exact time dynamics the system would exhibit noiselike fluctuations which never die but which decrease in amplitude with system size. We have seen that in our approximate KBE evolution the system, while being finite, attains a stationary state. Thus, for a system in which no narrow local resonances exist, the artificial damping of the KBE dynamics is expected to increasingly resemble the physical damping as the system grows. However, the situation is different when such sharp resonances do exist. If a sharp resonance is narrower than the width associated with the artificial damping, then it will be the latter that will dominate the system's temporal behavior in spite of the system's large size.

Self-consistency and damping. In MBPT, the self-energy accounts for possible excitations of the system which involve a certain number of particles/holes. Any self-consistent MBA with a frequency-dependent self-energy includes diagrams of all orders. These terms act as an effective bath which gives rise to infinitely many discrete poles in the ground state (in isolated systems) and correlation-induced damping in the time dynamics. In a finite system, there will be contributions to the self-energy which annihilate more holes/particles than those which can be accommodated in the system. In an exact
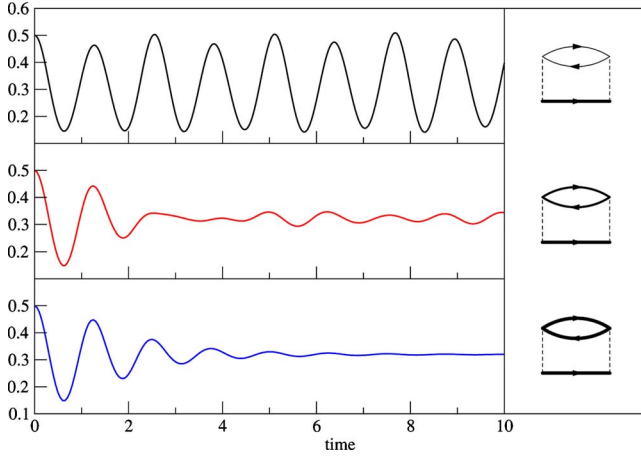
FIG. 16. (Color online) Time-dependent densities for Born approximations with different levels of self-consistency for M =2, n=1/2, U=1, w_0=5; BA$_0$ (black), BA$_{HFA}$ (red), and BA (blue). The time is given in units of the inverse hopping parameter of the central region, V^{-1}.

FIG. 17. (Color online) Time-dependent densities for a cluster isolated in the TMA with sudden and slow switch on for M =2, U=1, w_0=8. Sudden switch on (thin black), slow switch on (t_{max}=40) (thick red), and ground-state density of the final Hamiltonian (dashed red). The time is given in units of the inverse hopping parameter of the central region, V^{-1}.

theory, these unphysical terms would be exactly canceled, order by order, by other unphysical pieces. In approximations such as the GWA or the TMA, there is in general no such perfect compensation. The infinite number of poles of the ground state and the correlation-induced damping will thus be artificial for a finite system. Similar arguments are also valid for an infinite system. For any given volume in space, there will be a maximum number of particles which can be accommodated at a given time. For an extended system and/or if the interaction is long ranged the artificial contributions will, however, be much less pronounced.

In Fig. 16, we present results from three versions of the BA to illustrate the effect of an increasing level of self-consistency.[56] These approximations, which are all particle conserving,[57] involve different polarization propagators. In the first case we evaluate the polarization propagator with ground-state propagators (BA$_0$) (top panel). In this case, the density does not damp. In the second case, we evaluate the polarization with propagators in the time-dependent HFA approximation (BA$_{HFA}$) (middle panel). In this case, we observe partial damping. If we finally use the self-consistent G (BA) (bottom panel), we get complete damping. We see in other words that if all G's that build up the self-energy are the self-consistent ones we reach a steady state.[58]

Multiple steady states

Another striking feature related to the correlation-induced damping is that the steady state is not unique for a given final external field: it depends on how the perturbation is switched on, see Fig. 17. In our simulations, in the case of an adiabatic turn on $[w(t)=w_0t/t_{max}]$, we reach the ground state of a system with an on-site energy corresponding to the final external perturbation. This is consistent with the adiabatic theorem. If, however, the perturbation is switched on suddenly, we reach a nonphysical steady state with the same energy as at $t=0^+$. This nonuniqueness is indicative of an important aspect: given a final external potential, there are multiple, in
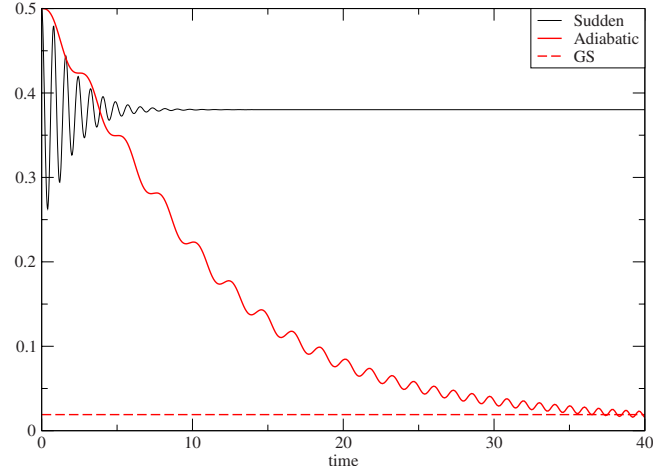
principle infinitely many, solutions of the stationary KBE in finite clusters.

The rise of different steady states during the time propagation can, somewhat heuristically, be understood as a history dependence of the occupation of the excited states. In other words, if we have an adiabatic switch on then only the lowest states will be populated but if the switch on is fast then also the higher energy states get populated.[59]

B. Contacted clusters: correlation-induced damping and quasisteady states

The phenomenology (and the reasons behind it) of the correlation-induced damping manifest in a similar way when the central region is coupled to macroscopic leads, where we have both a self-energy, Σ_{emb}, from the leads and a self-energy, Σ_{MBA}, from the interactions.

Both contributions are nonlocal in time and may lead to damping. Thus, in general we have two damping mechanisms: One due to the coupling to the continuous lead band and one induced by correlations.

In Fig. 18, we present the time-dependent densities within the TMA for a dimer, both isolated and coupled to unbiased leads,[60,61] subject to an external field with sudden and slow $[w(t)=w_0t/t_{max}]$ switch on; panel (a) and panel (b), respectively.[62]

Similarly to the isolated case, we find that for a slow switch on we tend to reach the ground state corresponding to the final Hamiltonian (given by the dashed curves) while for a sudden switch on, we reach another (quasi)steady state. With the term "quasisteady states" we mean long-lived excitations which can take an arbitrary long time to decay to the true steady state. When the strength of the perturbation is such that the ground state corresponding to the final external potential contains states outside the band continuum, the KBE give rise to multiple quasisteady states.[63] In practice it
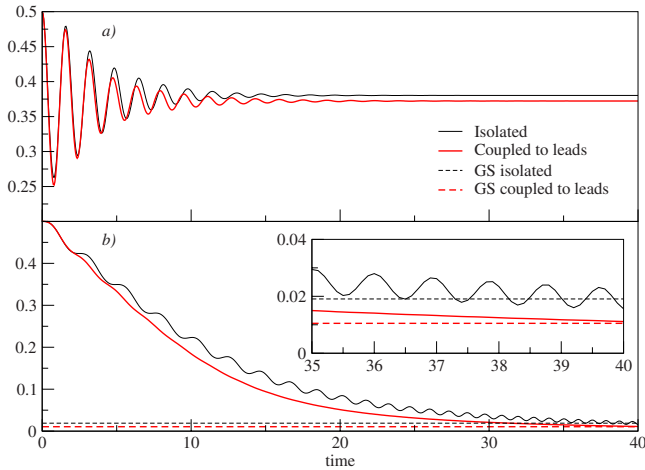
FIG. 18. (Color online) Time-dependent densities for a cluster isolated and coupled to two leads in the TMA with sudden and slow switch on. $M=2$, $U=1$, $w_0=8$. In the contacted case, the on-site energies $=-U/2$. Lead parameters: $V_{L_\alpha}=1$, $V_{L_\alpha C}=0.5$, filling $=0.5$, and bias $=0$. (a) Sudden switch on: isolated cluster (thin black), coupled to leads (thick red). (b) Slow switch on ($t_{max}=40$): isolated cluster (thin black), coupled to leads (thick red); ground-state densities of the final Hamiltonian: isolated cluster (dashed black), coupled to leads (dashed thick red). Inset: expanded view of the long-time limit behavior. The time is given in units of the inverse hopping parameter of the central region, V^{-1}.

means that it can be impossible, due to numerical limitations, to reach the true steady state by time evolution.[64] In all approximations which include correlation effects we have that the continuous nature of the band spreads out to all frequencies and thus the Σ_{MBA} will have a nonvanishing imaginary part in the whole spectrum. This imaginary part will, however, decrease very fast outside the band and therefore the lifetime of the states outside the band can be arbitrarily long depending on how far from the band they are.

The quasisteady states vary continuously with the way the final potential is reached. In other words there infinitely many quasisteady states where similar switch ons give similar quasisteady states. In the case of the HFA we see that the density continues to oscillate if we have more than one pole in the ground state of the final Hamiltonian. This results is consistent with recent work on the role of bound states in quantum transport.[65–68] However, we wish to remark that, in the HFA, the frequency, amplitude and average value of the oscillating density will, however, depend on the way the external field is switched on. In the case of $U=0$, however, the frequency is independent of the switch on.[66]

The damping induced by correlations and the one due to the coupling to the macroscopic contacts have in general different characteristic time scales. This is clearly seen in Fig. 19 where we have gradually increased the coupling to the leads: here, the external field and the lead bandwidth are such that the corresponding ground state of the final Hamiltonian contains no states outside the band continuum. In the case of an isolated cluster ($V_{L_\alpha C}=0$), the damping is only due to correlations. Once the coupling to the leads is nonzero, there will be, in addition to the correlation-induced one, a damping due to the contacts; the latter will eventually bring
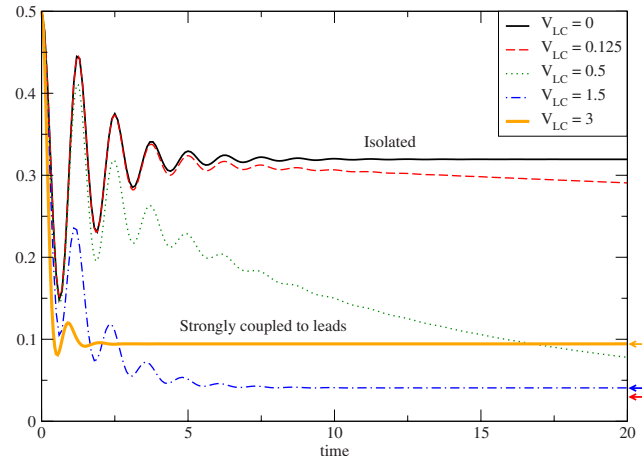
FIG. 19. (Color online) Time-dependent densities for a cluster with different couplings to two unbiased leads in the BA. $M=2$, $U=1$, on-site energies $=-U/2$, $w_0=5$, $V_{L_\alpha}=5$, and filling $=0.5$ in the leads. The time is given in units of the inverse hopping parameter of the central region, V^{-1}.

the system to the corresponding ground state. In Fig. 19, the ground-state values of the densities are represented by arrows (on the scale of the figure, the red and green arrows are not distinguishable). Note that each curve in Fig. 19 corresponds to a different system, i.e., with a different device-lead coupling strength. Each of these systems has a different final Hamiltonian, i.e., a different corresponding ground state. When the coupling strength is weak ($V_{L_\alpha C}=0.125, 0.5$), the time scale of the damping due to the leads is much longer than correlation-induced one. For intermediate coupling strengths ($V_{L_\alpha C}=1.5$), the characteristic times will be of the same order of magnitude and the interplay of the two mechanisms becomes intrinsically difficult to discern. When the coupling strength is strong ($V_{L_\alpha C}=3$), the damping is completely dominated by the leads.

As a final remark, we know that the correlation-induced damping is artificial in isolated clusters, and we saw in Fig. 19 that when the coupling to the leads is weak, the initial damping is also dominated by correlations. These two facts together seem to cast some doubt on the capability of the KBE+MBAs scheme to describe (within the simple MBAs discuss here) transients in the weak coupling case (a regime which is of high experimental interest, and in fact among the most investigated in the literature).

To summarize this section, we see that the correlation-induced damping is present both in isolated and contacted clusters whenever approximations involving correlation effects are used. If there are sharp resonances (infinitely sharp in the case of isolated clusters), there will be multiple steady states, in isolated clusters, or quasisteady states in clusters coupled to leads. For isolated clusters, this damping is artificial as the exact solution does not reach a steady state. The question whether or not the correlation-induced damping and the existence of multiple quasisteady states in a cluster coupled to leads are an artifact of MBPT or are instead physical properties of this model is left to future work.

XI. CONCLUSIONS AND OUTLOOK

A main objective of this paper has been to describe in detail a method, within the framework of the time-dependent KBEs, to study finite systems in equilibrium as well as out of equilibrium. The main emphasis of the paper has been on finite clusters, for which a meromorphic representation of the equilibrium many-body quantities is possible, but, in few instances, we have also considered some results for contacted clusters.

As a concrete application, we examined the time evolution of clusters with strong, short-ranged electron interactions within several MBAs, and compared the results to exact ones. A first main outcome of these comparisons is that, for short-ranged, Hubbard-type interactions, the T-matrix approximation performs very well at low densities, and is in general superior to the GW and second Born approximations, both in describing the time-dependent density and the corresponding exchange-correlation potential.

A second important outcome of our work is the existence of two remarkable features of the time-dependent KBE. The first is that the KBE present a correlation-induced damping in the nonlinear regime. The second is that the steady state reached for isolated clusters is not unique, i.e., the stationary KBE support multiple stationary states. In the case of clusters coupled to macroscopic leads the KBE will yield multiple quasisteady states with arbitrarily long lifetimes if there are sharp resonances outside the band continuum. Since a finite cluster subject to a nonadiabatic perturbation will oscillate indefinitely, it is clear that, for finite systems, such damping and multiple steady-state behavior are artificial. We argue that these shortcomings will always be present when applying infinite order perturbation theory, with self-energies which are nonlocal in time, to finite systems. In this paper, we were not able to provide a conclusive answer to which extent these two aspects of the KBE bear a physical meaning, or if they are a spurious effect of MBPT.

Future research activity may be envisaged in various directions. On the methodological side, it would be of interest to further investigate, for contacted systems, if the correlation-induced damping and the multiple quasisteady states are physical for model Hamiltonians of the kind investigated here.[69] A second methodological issue we are currently addressing is the performance of the different MBAs in quantum transport geometries. We will do by comparing the approximate results with those of time-dependent density-matrix renormalization-group calculations.[70] Another possible line of study would be searching for algorithms to reduce/optimize the computational costs of time-dependent KBE numerical calculations. This is necessary to deal with more realistic systems. As a fourth direction, it would be of great interest to study the effect of including bosonic degrees of freedom as vibration phenomena often play an crucial role in quantum transport. Finally, we also intend to use our KBE-based computational treatments in some specific applications: Possible examples are real-time qubit manipulation, bistability induced by electron-phonon interaction, and cold-atom dynamics. More specific details are deferred to future publications.

ACKNOWLEDGMENTS

APPENDIX A: ENERGY FUNCTIONALS

The energy functionals considered here are the Galitskii-Migdal (GM) and the Luttinger-Ward (LW). An important difference between them is that the GM needs only the knowledge of the single-particle Hamiltonian and of the spectral function of G while the LW incorporates the Φ functional as well as $\Sigma[G]$, which depends on which approximation one is using. Here we give the expression for the LW functional for the GW approximation. In practice, we evaluated the LW only in the ground state, i.e., in frequency space, while the GM was also used during time evolution.

1. Galitskii-Migdal

In frequency space, the GM functional reads[71]

$$E = -\frac{i}{2}\text{Tr}\{(\epsilon + h)G\}, \quad (A1)$$

where Tr stands for trace[72] and h is the single-particle Hamiltonian *not* including Σ_{HF}. Thus

$$E = \sum_R \sum_{i=1}^{n_F} a_i A_{RR}^i - \sum_{RR'} \sum_{i=1}^{n_F} A_{RR'}^i h_{RR'}, \quad (A2)$$

where n_F is the number of poles below the Fermi energy, and after having made use of the meromorphic representation of $G^<$. In time space, the form of E becomes

$$E = -\frac{i}{2}\text{Tr}[(i\partial_t + h)G^<(t,t^+)]. \quad (A3)$$

Making use of the equation of for G, we obtain

$$E = -\frac{i}{2}\text{Tr}[hG^<(t,t^+)] - \frac{i}{2}\text{Tr}[(h + \Sigma_{HF})G^<(t,t^+) + I_1^<(t,t^+)]. \quad (A4)$$

2. Luttinger-Ward

The LW energy functional is[73]

$$iE = \Phi - \text{Tr}\{\Sigma G + \ln(\Sigma - G_0^{-1})\}, \quad (A5)$$

where the self-energy depends functionally on the input G i.e., $\Sigma = \Sigma[G]$ and Φ is the generating (of the MBAs) functional. Specializing to the case of the GW approximation, the Φ functional becomes

$$\Phi_{GW} = \Phi_{HF} + \frac{1}{4}\text{Tr}\{\ln[1 - UP] + UP\}, \quad (A6)$$

where $\Phi_{HF} = (i/2)\text{Tr}\{\Sigma_{HF}[G]G\}$. When computing the logarithmic term $\ln(\Sigma - G_0^{-1})$ in Eq. (A5), it is useful to make the following separation:

$$\ln[\Sigma - G_0^{-1}] = \ln[-G_{HF}^{-1}] + \ln[1 - G_{HF}\Sigma_c], \qquad (A7)$$

where $G_{HF}^{-1} = \epsilon - \mathfrak{h}$ and $\mathfrak{h}$ incorporates the Hartree and Fock terms and where Σ_c is the correlation part of the GW self-energy. The first term in Eq. (A7) is the sum of the eigenvalues of the occupied Hartree-Fock single-particle states (calculated from the correlated Green's function) which obviously does not correspond to the Hartree-Fock energy. The second contribution in Eq. (A7) can be evaluated with a well-known identity,[74]

$$\ln[1 - G_{HF}\Sigma_c] = -\int_0^1 \frac{G_{HF}\Sigma_c}{1 - \lambda G_{HF}\Sigma_c}d\lambda = -\int_0^1 \widetilde{G}\Sigma_c d\lambda. \qquad (A8)$$

In Eq. (A8), $\widetilde{G}$ satisfies the Dyson equation,

$$\widetilde{G} = G_{HF} + \lambda G_{HF}\Sigma_c\widetilde{G}. \qquad (A9)$$

The other logarithmic term in Φ_{GW}, i.e., $\ln[1 - UP]$, is treated in a similar way. In the actual calculation, expressions of the form $\text{Tr}[AB]$ are evaluated analytically, while integrals of the kind $\int_0^1 AB d\lambda$ are performed numerically.

APPENDIX B: TIME PROPAGATION ALGORITHM

To increase the numerical stability of the time propagation, we incorporate the time-local part of the self-energy into the noninteracting Hamiltonian ($\mathfrak{h} = h + \Sigma_{HF}$). The evolution from this modified single-particle Hamiltonian can be expressed in terms of a single-particle evolution operator S which is a time-dependent matrix in single-particle labels. The Green's function can thus be reexpressed via a unitary-gauge-transformed image,

$$G^{\lessgtr}(t_1,t_2) = S(t_1,0)g^{\lessgtr}(t_1,t_2)S^{\dagger}(t_2,0), \qquad (B1)$$

where S satisfies the following differential equation:

$$i\partial_{t_1}S(t_1,0) = \mathfrak{h}(t_1)S(t_1,0) \qquad (B2)$$

with the initial condition

$$S(0,0) = S^{\dagger}(0,0) = 1 \qquad (B3)$$

and the group property

$$S(t_1,\bar{t})S(\bar{t},t_2) = S(t_1,t_2). \qquad (B4)$$

Specializing to the case of $G^>$, we get

$$\begin{aligned} i\partial_{t_1}G^>(t_1,t_2) &= \mathfrak{h}(t_1)S(t_1,0)g^>(t_1,t_2)S^{\dagger}(t_2,0) \\ &\quad + S(t_1,0)i\partial_{t_1}g^>(t_1,t_2)S^{\dagger}(t_2,0) \\ &= \mathfrak{h}(t_1)G^>(t_1,t_2) + I_1^>(t_1,t_2), \qquad (B5) \end{aligned}$$

where the second equality comes from the Kadanoff-Baym equation for $G^>$. This results in

$$i\partial_{t_1}g^>(t_1,t_2) = S^{\dagger}(t_1,0)I_1^>(t_1,t_2)S(t_2,0). \qquad (B6)$$

Therefore, by integrating from present time T_p to $T_p + \Delta$,

$$\begin{aligned} i[g^>(T_p + \Delta, t_2) &- g^>(T_p,t_2)] \\ &= \int_{T_p}^{T_p+\Delta} S^{\dagger}(\bar{t},0)I_1^>(\bar{t},t_2)S(t_2,0)d\bar{t} \\ &= S^{\dagger}(T_p,0)\int_0^{\Delta} S^{\dagger}(\bar{t}+T_p,T_p)I_1^>(\bar{t}+T_p,t_2)S(t_2,0)d\bar{t}. \end{aligned}$$
$$(B7)$$

Thus

$$\begin{aligned} G^>(T_p + \Delta, t_2) &= S(T_p + \Delta, T_p)G^>(T_p,t_2) \\ &\quad - iS(T_p + \Delta, T_p)\int_0^{\Delta} S^{\dagger}(\bar{t}+T_p,T_p) \\ &\quad \times I_1^>(\bar{t}+T_p,t_2)d\bar{t}. \qquad (B8) \end{aligned}$$

Up to this point we have not made any approximations but merely formal rewritings of the KBE. To calculate the $S(T_p + \Delta, T_p)$, we divide the interval $[T_p, T_p + \Delta]$ into N intervals in which the single-particle Hamiltonian, $\mathfrak{h}$, is taken constant and evaluated at the midpoint. For a constant $\mathfrak{h}$, we obtain

$$S\left[T_p + \frac{(j+1)\Delta}{N}, T_p + \frac{j\Delta}{N}\right] = \exp\left\{-i\mathfrak{h}\left[T_p + \frac{(j+1/2)\Delta}{N}\right]\frac{\Delta}{N}\right\}, \qquad (B9)$$

which is evaluated by diagonalization. The resulting expression becomes

$$S(T_p + \Delta, T_p) = \prod_{j=0}^{N-1} \exp\left\{-i\mathfrak{h}\left[T_p + \frac{(j+1/2)\Delta}{N}\right]\frac{\Delta}{N}\right\}. \qquad (B10)$$

Given that N is taken large enough, the only error of the above expression comes from the extrapolation/interpolation of $\mathfrak{h}$ (done with a four-point formula). This error is in general very small as the density (which enters $\mathfrak{h}$ via the HF term) is a continuous and smooth function of time.

To solve Eq. (B8) we also need to approximate the integral. This can be done in two different ways depending on which of the two quantities $I_1^>(\bar{t}+T_p,t_2)$ or $\widetilde{I}_1^>(\bar{t}+T_p,t_2) = S^{\dagger}(\bar{t}+T_p,T_p)I_1^>(\bar{t}+T_p,t_2)$ is the most slowly varying function. We have tried both and seen that the $\widetilde{I}_1^>(\bar{t}+T_p,t_2)$ is the smoothest. The integral is done numerically, typically with a two- or four-point formula. We have implemented both methods but for the systems we have studied we have not seen dramatic improvement. Similar expressions are used for the other KBE. Special attention is needed only for the time diagonal. In this case we combine the two first KBE, Eqs. (53) and (54) and using the property in Eq. (63),

$$i[\partial_{t_1} + \partial_{t_2}]G^<(t_1,t_2) = [\mathfrak{h}, G^<(t_1,t_2)] + I_1^<(t_1,t_2) - I_2^<(t_1,t_2), \qquad (B11)$$

we then change to the variables $t = (t_1+t_2)/2$ and $t' = t_1 - t_2$. This gives

$$i\partial_t G^<(t+t'/2, t-t'/2) = [\hbar, G^<(t+t'/2, t-t'/2)]$$
$$+ I_1^<(t+t'/2, t-t'/2)$$
$$- I_2^<(t+t'/2, t-t'/2). \quad \text{(B12)}$$

By performing the same gauge transformation as above and setting $t' = t_1 - t_2 = 0$, we obtain[75]

$$i\partial_t g^<(t) = \widetilde{I}_1^<(t) - \widetilde{I}_2^<(t), \quad \text{(B13)}$$

where $\widetilde{I}^<(t) = S^\dagger(t,0) I^<(t,t) S(t,0)$. Integrating from time T_p to $T_p + \Delta$, we obtain

$$g^<(T_p + \Delta) = g^<(T_p) - i \int_{T_p}^{T_p+\Delta} [\widetilde{I}_1^<(\bar{t}) - \widetilde{I}_2^<(\bar{t})] d\bar{t}, \quad \text{(B14)}$$

which leads to

$$G^<(T_p + \Delta) = S(T_p + \Delta, T_p) G^<(T_p) S^\dagger(T_p + \Delta, T_p)$$
$$- iS(T_p + \Delta, T_p) \int_0^\Delta (\widetilde{I}_1^<(\bar{t} + T_p) - \widetilde{I}_2^<(\bar{t} + T_p)) d\bar{t}$$
$$\times S^\dagger(T_p + \Delta, T_p). \quad \text{(B15)}$$

The integral is then evaluated in the same way as discussed above for the case $t_1 \neq t_2$.

[1] L. P. Kadanoff and G. Baym, *Quantum Statistical Mechanics* (Benjamin, New York, 1962).

[2] L. V. Keldysh, Zh. Eksp. Teor. Fiz. **47**, 1515 (1964) [Sov. Phys. JETP **20**, 1018 (1965)].

[3] P. Danielewicz, Ann. Phys. **152**, 239 (1984).

[4] See, for example, *Progress in Nonequilibrium Green's Functions III*, J. Phys. Conf. Ser. Vol. 35, edited by M. Bonitz and A. Filinov (Institute of Physics, Bristol, 2006).

[5] N.-H. Kwong and M. Bonitz, Phys. Rev. Lett. **84**, 1768 (2000).

[6] A. P. Jauho, in *Progress in Nonequilibrium Green's Functions III*, J. Phys. Conf. Ser. Vol. 35, edited by M. Bonitz and A. Filinov (Ref. 4), p. 313.

[7] G. Stefanucci and C.-O. Almbladh, Phys. Rev. B **69**, 195318 (2004).

[8] N. E. Dahlen, R. van Leeuwen, and A. Stan in *Progress in Nonequilibrium Green's Functions III*, J. Phys. Conf. Ser. Vol. 35, edited by M. Bonitz and A. Filinov (Ref. 4), p. 340.

[9] K. Balzer, M. Bonitz, R. van Leeuwen, A. Stan, and N. E. Dahlen, Phys. Rev. B **79**, 245306 (2009).

[10] M. Galperin, A. Nitzan, and M. A. Ratner, Phys. Rev. B **76**, 035301 (2007).

[11] K. S. Thygesen and A. Rubio, Phys. Rev. B **77**, 115333 (2008).

[12] P. Darancet, A. Ferretti, D. Mayou, and V. Olevano, Phys. Rev. B **75**, 075102 (2007).

[13] P. Myöhänen, A. Stan, G. Stefanucci, and R. van Leeuwen, EPL **84**, 67001 (2008).

[14] P. Myöhänen, A. Stan, G. Stefanucci, and R. van Leeuwen, Phys. Rev. B **80**, 115107 (2009).

[15] A.-M. Uimonen, E. Khosravi, G. Stefanucci, S. Kurth, R. van Leeuwen, and E. K. U. Gross, in *Progress in Nonequilibrium Green's Functions IV*, J. Phys.: Conf. Ser. **220**, 012018 (2010).

[16] J. K. Freericks, Phys. Rev. B **77**, 075109 (2008).

[17] M. Puig von Friesen, C. Verdozzi, and C.-O. Almbladh, Phys. Rev. Lett. **103**, 176404 (2009).

[18] See, for example, T. H. Oosterkamp, T. Fujisawa, W. G. van der Wiel, K. Ishibashi, R. V. Hijman, S. Tarucha, and L. P. Kouwenhoven, Nature (London) **395**, 873 (1998).

[19] B. T. Seaman, M. Kramer, D. Z. Anderson, and M. J. Holland, Phys. Rev. A **75**, 023615 (2007).

[20] A short account of this work was reported previously (Ref. 17).

[21] L. Hedin, Phys. Rev. **139**, A796 (1965).

[22] V. Galitskii, Sov. Phys. JETP **7**, 104 (1958).

[23] D. Semkat, D. Kremp, and M. Bonitz, Contrib. Plasma Phys. **42**, 31 (2002).

[24] K. S. Thygesen, Phys. Rev. Lett. **100**, 166804 (2008).

[25] P. Romaniello, D. Sangalli, J. A. Berger, F. Sottile, L. G. Molinari, L. Reining, and G. Onida, J. Chem. Phys. **130**, 044108 (2009).

[26] W. Nelson, P. Bokes, P. Rinke, and R. W. Godby, Phys. Rev. A **75**, 032505 (2007).

[27] E. Runge and E. K. U. Gross, Phys. Rev. Lett. **52**, 997 (1984).

[28] R. van Leeuwen, N. E. Dahlen, G. Stefanucci, C. O. Almbladh, and U. von Barth, *Time-Dependent Density Functional Theory* (Springer, New York, 2006) (and references therein).

[29] C. Verdozzi, Phys. Rev. Lett. **101**, 166401 (2008).

[30] This condition also applies to the first argument.

[31] In extended Coulomb systems, w and the Hartree potential Σ_H are infinite but with a finite sum and must be treated together. In this work, we consider model systems with short-range interactions and such a procedure is not mandatory.

[32] In Ref. 17, the concept of "partial summations" is used to describe approximations beyond HFA, i.e., with a self-energy involving correlation effects.

[33] In the spin-independent treatment $P = \Sigma_\sigma P_\sigma$.

[34] There exist also contributions coming from ladder diagrams with interactions only/also in the electron-hole channel, usually of principal relevance in exciton-type problems; however, such contributions are not the dominant ones in the low-density limit for our Hubbard clusters with one orbital/site; and in the rest of the paper, we do not consider them altogether, limiting ourselves to particle-particle or hole-hole ladder contributions.

[35] S. Datta, *Electronic Transport in Mesoscopic Systems* (Cambridge University Press, Cambridge, 1995).

[36] H. Haug and A.-P. Jauho, *Quantum Kinetics in Transport and Optics of Semiconductors* (Springer, Berlin, 1996).

[37] M. Cini and C. Verdozzi, Nuovo Cimento D **9**, 1 (1987).

[38] The Dyson equations for T or W are solved in a similar way.

[39] In the case of complex time arguments we would have $G(12) = -G(2^*1^*)^\dagger$. This will henceforth be implicit in all similar symmetry relations.

[40] The $T^>(t,t)$ is also needed as there is no closed relation to $T^<(t,t)$.

[41] H. S. Köhler, N. H. Kwong, and H. A. Yousif, Comput. Phys. Commun. **123**, 123 (1999).

[42] W. Ku and A. G. Eguiluz, Phys. Rev. Lett. **89**,126401 (2002); or W. Ku, Ph.D. thesis, The University of Tennessee, 2000.

[43] In general, it would correspond to the occupation numbers of the single-particle basis.

[44] A. Stan, N. E. Dahlen, and R. van Leeuwen, J. Chem. Phys. **130**, 224101 (2009).

[45] E. H. Lieb and F. Y. Wu, Phys. Rev. Lett. **20**, 1445 (1968).

[46] C.-O Almbladh, in Ref. 4, p. 127.

[47] B. Holm and U. von Barth, Phys. Rev. B **57**, 2108 (1998).

[48] Continuous broadened ground-state spectral functions have been found for few electron quantum dots (Ref. 9), in contrast, for the systems considered here our results show only discrete spectral features.

[49] W. Li, G. Xianlong, C. Kollath, and M. Polini, Phys. Rev. B **78**, 195109 (2008).

[50] C.-O. Almbladh, U. von Barth, and R. van Leeuwen, Int. J. Mod. Phys. B **13**, 535 (1999).

[51] U. von Barth, N. E. Dahlen, R. van Leeuwen, and G. Stefanucci, Phys. Rev. B **72**, 235109 (2005).

[52] R. van Leeuwen, Phys. Rev. Lett. **76**, 3610 (1996).

[53] C. Verdozzi, R. W. Godby, and S. Holloway, Phys. Rev. Lett. **74**, 2327 (1995).

[54] In a steady state, all the single-particle properties are independent of time and the one-particle Green's function depends only on the time difference, i.e., $G(t,t') \rightarrow G(t-t')$. We alert the reader that this definition encompasses isolated and (unbiased/biased) contacted systems alike.

[55] Initializing with G_0 corresponds to a sudden switch on of the interaction as well as of the external field.

[56] The different BAs are done using a spin-dependent treatment, which is equivalent to the spin-independent one only when done fully self-consistently.

[57] U. von Barth (unpublished).

[58] This conclusion applies to all MBAs here, although partially self-consistent but particle-conserving schemes can be easily devised for GWA but not for TMA.

[59] Olov Karlström and Elham Khosravi (private communication).

[60] The theoretical formulation to treat macroscopic leads within the Keldysh formalism will be presented in detail in a future paper.

[61] The hopping parameter in the central region is, similarly to the isolated case, set to unity throughout the paper.

[62] In Figs. 18 and 19, we have, in addition to a nonzero external field shifted the on-site energy by $-U/2$ in order to have the same filling in the central region as in the isolated clusters.

[63] The existence of long-lived quasisteady states remains valid in the case that we apply a bias to the leads. In that case the quasisteady state will depend both on how the external field and the bias is switched on.

[64] When no bias is applied then the true steady state corresponds to the final ground state. In general, when a bias is applied it is plausible that there will be only one true steady state.

[65] A. Dhar and D. Sen, Phys. Rev. B **73**, 085119 (2006).

[66] G. Stefanucci, Phys. Rev. B **75**, 195115 (2007).

[67] For a review, see E. Khosravi, S. Kurth, G. Stefanucci, and E. K. U. Gross, Appl. Phys. A **93**, 355 (2008).

[68] C. Verdozzi, G. Stefanucci, and C.-O. Almbladh, Phys. Rev. Lett. **97**, 046603 (2006). In this paper, of a self-consistent oscillatory solution was observed in a short wire with Holstein-type phonons, and connected to 1D noninteracting leads.

[69] Should these features of the KBE turn out to be artificial, one could try to find ways to suppress the nonphysical behavior while keeping the connection to MBPT. One possibility could be to use the variational properties of the underlying Φ functional and use the Sham-Schlüter equation to determine on the fly the corresponding TDDFT potentials. At full self-consistency, the TDDFT dynamics would just reproduce the damped KBE dynamics. If one instead use optimized one-particle G when constructing the exchange correlation potential, v_{xc}.(Refs. 50 and 51), we expect that the nonphysical damping will be reduced or removed without seriously deteriorating the short-time dynamics. In the BA, this approach consists in using a (time-) optimized independent-particle G when constructing the self-energy and v_{xc} and in Sec. X we saw that the damping is indeed reduced. The use of MBPT based TDDFT potentials could also be of great importance, due to the possibility of treating larger and more complex systems.

[70] See, for example, P. Schmitteckert, Phys. Rev. B **70**, 121302(R) (2004).

[71] V. M. Galitskii and A. B. Migdal, Zh. Eksp. Teor. Fiz. **34**, 139 (1958) [Sov. Phys. JETP **139**, 96 (1958)].

[72] In frequency space $\text{Tr} \equiv 2 \lim_{\eta \to 0^+} \Sigma_{RR'} \delta_{RR'} \int \frac{d\epsilon}{2\pi} e^{i\epsilon\eta}$ and in time space $\text{Tr} \equiv 2\Sigma_{RR'} \delta_{RR'}$. The space in which the expressions are represented are given by the context.

[73] J. M. Luttinger and J. C. Ward, Phys. Rev. **118**, 1417 (1960).

[74] P. Güttinger, Z. Phys. **73**, 169 (1932).

[75] Explicit reference to the two-time dependencies is omitted as $t_1 = t_2$.